APPENDIX C

ACTIVE-FRACTURE CONCEPT IN THE UNSATURATED ZONE TRANSPORT MODEL (RESPONSE TO TSPAI 3.28 AND TSPAI 3.29)

Note Regarding the Status of Supporting Technical Information

This document was prepared using the most current information available at the time of its development. This Technical Basis Document and its appendices providing Key Technical Issue Agreement responses that were prepared using preliminary or draft information reflect the status of the Yucca Mountain Project's scientific and design bases at the time of submittal. In some cases this involved the use of draft Analysis and Model Reports (AMRs) and other draft references whose contents may change with time. Information that evolves through subsequent revisions of the AMRs and other references will be reflected in the License Application (LA) as the approved analyses of record at the time of LA submittal. Consequently, the Project will not routinely update either this Technical Basis Document or its Key Technical Issue Agreement appendices to reflect changes in the supporting references prior to submittal of the LA.

APPENDIX C

ACTIVE-FRACTURE CONCEPT IN THE UNSATURATED ZONE TRANSPORT MODEL (RESPONSE TO TSPAI 3.28 AND TSPAI 3.29)

This appendix provides a response for Key Technical Issue (KTI) agreements Total System Performance Assessment and Integration (TSPAI) 3.28 and 3.29. These agreements relate to the use of the active-fracture concept in the unsaturated zone transport model.

C.1 KEY TECHNICAL ISSUE AGREEMENTS

C.1.1 TSPAI 3.28 and TSPAI 3.29

Agreements TSPAI 3.28 and 3.29 were reached during the U.S. Nuclear Regulatory Commission (NRC)/U.S. Department of Energy (DOE) Technical Exchange and Management Meeting on Total System Performance Assessment and Integration held August 6 to 10, 2001, in Las Vegas, Nevada. TSPAI Subissue 3, Model Abstraction, UZ3—Radionuclide Transport in the Unsaturated Zone, was discussed at that meeting (Reamer 2001 [DIRS 165171]). No submittal related to these KTI agreements has been made to the NRC.

Subsequent to the agreements, NRC staff concerns underlying TSPAI 3.28 and 3.29 were recorded in *Integrated Issue Resolution Status Report* (NRC 2002 [DIRS 159538], p. 3.3.7-5 and pp. 3.3.7-17 to 3.3.7-18). These concerns mean that, in addition to the language of the agreements (Reamer 2001 [DIRS 165171]), there is a general need for improved transparency of model parameter estimation and numerical implementation of the abstraction transport model, based on information provided in *Particle Tracking Model and Abstraction of Transport Processes* (CRWMS M&O 2000 [DIRS 141418]) and *Unsaturated Zone Flow and Transport Model Process Model Report* (CRWMS M&O 2000 [DIRS 151940]). These reports specifically require clarification of the methods of estimating fracture porosity, fracture–matrix connection area, fracture aperture values (and whether they have been adjusted to account for the active-fracture concept), and fracture spacing. The method of implementing the active-fracture concept in the abstraction transport model also requires clarification, including whether or not the fraction of active fractures is factored into the calculation of fluid velocity in the transport model.

The wording of the agreements is as follows:

TSPAI 3.28

> DOE needs to provide independent lines of evidence to provide additional confidence in the use of the active-fracture continuum concept in the transport model (UZ3.5.1). DOE will provide independent lines of evidence to provide additional confidence in the use of the active fracture continuum concept in the transport model. This will be documented in Radionuclide Transport Models under Ambient Conditions AMR (MDL-NBS-HS-000008) and Unsaturated Zone Flow Models and Submodels AMR (MDL-NBS-HS-000006) expected to be available to NRC in FY 2003.

TSPAI 3.29

Provide verification that the integration of the active fracture model with matrix diffusion in the transport model is properly implemented in the TSPA abstraction (UZ3.TT.3). DOE will provide verification that the integration of the active fracture model with matrix diffusion in the transport model is properly implemented in the TSPA abstraction. This verification will be documented in the Particle Tracking Model and Abstraction of Transport Processes (ANL-NBS-HS-000026) expected to be available to NRC in FY 2003.

C.1.2 Related Key Technical Issue Agreements

None.

C.2 RELEVANCE TO REPOSITORY PERFORMANCE

The unsaturated zone is an important natural barrier for the performance of the repository system at Yucca Mountain. The active-fracture concept is an important element of the unsaturated zone transport model, which is used primarily to represent the function of the unsaturated zone barrier below the repository in limiting transport from the drift invert to the saturated zone. The abstraction of the unsaturated zone transport model directly supports total system performance assessment (TSPA).

C.3 RESPONSE

Both TSPAI 3.28 and 3.29 relate to the use of the active-fracture model for TSPA. This response is guided by both the original language of the agreements (Reamer 2001 [DIRS 165171]) and the summary of concerns described in Section C.1.1.

Since agreements TSPAI 3.28 and 3.29 were reached in 2001, and due to subsequent discussions in the *Integrated Issue Resolution Status Report* (NRC 2002 [DIRS 159538]), the following model reports have been revised:

- *UZ Flow Models and Submodels* (BSC 2003 [DIRS 163045])
- *Analysis of Hydrologic Properties Data* (BSC 2003 [DIRS 161773])
- *Radionuclide Transport Models Under Ambient Conditions* (BSC 2003 [DIRS 163228])
- *Particle Tracking Model and Abstraction of Transport Processes* (BSC 2004 [DIRS 162730])
- *Calibrated Properties Model* (BSC 2003 [DIRS 160240]).

These revisions provide independent lines of evidence that improve confidence in the active-fracture model, verify the implementation of the active-fracture model with matrix diffusion in the total system performance for the license application (TSPA-LA) abstraction and improve transparency of implementation.

C.3.1 Independent Lines of Evidence for Additional Confidence in Active-Fracture Model (TSPAI 3.28)

In the active-fracture model conceptualization (Liu et al. 1998 [DIRS 105729], pp. 2,638 to 2,641), only a portion of the fractures in a fracture network are active (i.e., hydraulically conductive) under unsaturated conditions. The active portion is defined as a function of water saturation, S_e to the power of the active-fracture parameter _ (where _ is greater than or equal to 0 and less than or equal to 1) (Liu et al. 1998 [DIRS 105729], pp. 2,638 to 2,641). A _ value of 0 or a S_e value of 1 (corresponding to saturated conditions) indicates all fractures are active, while a _ value of 1 indicates the smallest active-fracture portion for a given saturation. The active-fracture model requires reformulation of the fracture–matrix interface area and the relative permeability and capillary pressure functions of the fracture (BSC 2003 [DIRS 163045], Section 6.8).

Evidence in support of the active-fracture model comes from the comparison of transport simulations with field data. These cases are summarized below and discussed in detail in Section C.4.1.

Groundwater Age Predictions Compared to ^{14}C Measurements–The sensitivity of groundwater age predictions to the active-fracture model parameter, _, was evaluated in one-dimensional numerical simulations. A range of _ values of 0.2 to 0.4 provided the best fit to borehole ^{14}C data in the TSw unit (BSC 2003 [DIRS 161773], pp. 78 to 82). Subsequent testing of a three-dimensional transport model (BSC 2003 [DIRS 163045], Section 7.5) showed that a _ value equal to the higher value from the range in the one-dimensional study (0.4) provided the best fit to the borehole groundwater age data.

Simulation of Fraction of Active Fractures Compared to Mineral Fracture Coating Data–Fracture coating data provide additional confidence that the active-fracture model appropriately describes water flow in fracture networks (BSC 2003 [DIRS 161773], Section 7.2.2). The presence of mineral coating on only a portion of the fractures along the Exploratory Studies Facility (ESF) shows that not all fractures transmit water, strongly supporting the concept of the active-fracture model. Furthermore, the estimated number of active fractures predicted from active-fracture model simulations based on the active-fracture model is consistent with measured values. Finally, these predictions used the same range of _ values used to fit the ^{14}C data, providing additional confidence in the active-fracture model.

Consistency Between Active-Fracture Model and Fractal Flow Patterns–Unsaturated flow patterns in a fracture network can be fractal. *Analysis of Hydrologic Properties Data* (BSC 2003 [DIRS 161773], Section 6.7) shows that the frequency of fractures having mineral coating in the ESF is consistent with a fractal flow pattern in the fracture network. A correspondence between _ and the fractal dimension of the flow system shows that the active-fracture model is theoretically consistent with fractal flow behavior in an unsaturated fracture network.

Final Comments–For a field test to provide independent evidence supporting the active-fracture model, it must be performed for the conditions that the active-fracture model describes, which is a fracture network, and include a large range of fracture saturations. The testing in Alcove 8–Niche 3 (also referred to as Niche 3107) performed to-date measured transport mainly

through a fault (see Section 5.3.4), which is geometrically distinct from a fracture network and is therefore not a good test of the active fracture model. *Radionuclide Transport Models Under Ambient Conditions* (BSC 2003 [DIRS 163228]) states that further testing in Yucca Mountain tuffs, under unsaturated conditions with multiple tracers, could significantly strengthen the validation arguments. Because field data are relatively sparse and support the active fracture model only indirectly, TSPA modeling uses a range of active fracture model parameters from three infiltration scenarios, as described in the next section.

C.3.2 Sources and Estimation Methods of Abstraction Transport Model Parameters (TSPAI 3.28 and 3.29)

Input Parameters for Rock Properties for Abstraction Model–The sources for rock properties for the abstraction model are listed in *Particle Tracking Model and Abstraction of Transport Processes* (BSC 2004 [DIRS 162730]) (see Table C-1). These include fracture porosity, fracture frequency, active-fracture model parameters, and fracture aperture. The use of these parameters is summarized in Section C.4.2.1.

Table C-1. Input Parameters

Parameter Name	Parameter Source	Parameter Values	Units	Distribution (or single value if fixed)
Fracture porosity	BSC 2003 [DIRS 161773]	Varies from layer to layer	None	_ distribution. Layers are grouped together based on similar rock properties.
Fracture frequency	BSC 2003 [DIRS 161773]	Varies from layer to layer	1/m	Log-normal distribution
Active-fracture model parameters	BSC 2003 [DIRS 163045]	Varies from layer to layer and with infiltration scenario	None	Fixed value for a specific infiltration
Fracture residual saturation	BSC 2003 [DIRS 160240]	0.01	None	Fixed
Fracture spacing and aperture	BSC 2003 [DIRS 161773]	Varies from layer to layer	m	Layers with similar rock properties are grouped together and the parameters are sampled.
Matrix diffusion coefficient	BSC 2003 [DIRS 164889]	Sampled parameter values	m^2/s	Layers are grouped together based on similar rock properties and parameters are sampled for estimating matrix diffusion coefficient.

NOTE: Citations can be found in *Particle Tracking Model and Abstraction of Transport Processes* (BSC 2004 [DIRS 162730]); extracted from *Particle Tracking Model and Abstraction of Transport Processes* (BSC 2004 [DIRS 162730], Section 4, Table 4-2).

Porosity Measurements–Porosity measurements are derived from gas tracer test data for one model layer. Observations of fracture geometry in the ESF are used to apply the porosity values derived from the gas tracer test data to other units (BSC 2003 [DIRS 161773], Section 6.1.3). The methodology for obtaining porosity values is discussed in detail in Section C.4.2.2.

Development of Fracture Properties from Field Data–*Analysis of Hydrologic Properties Data* (BSC 2003 [DIRS 161773], Section 6.1.2) documents the development of fracture properties

(i.e., fracture frequency, intensity, fracture interface area, and aperture) from field data. This is summarized in Section C.4.2.3.

Fracture Aperture, Porosity, and Frequency Data in Abstraction Model–Fracture porosity and frequency data (the inverse of fracture spacing) are sampled from a mean and standard deviation for each group of values in order to account for parameter uncertainty (BSC 2004 [DIRS 162730], Section 6.5.7). Fracture apertures in the abstraction model are computed from a relationship between sampled fracture porosity and frequency (BSC 2004 [DIRS 162730], Section 6.5.7). This is summarized in Section C.4.2.4.

Residual Saturation and the Active-Fracture Model _ Parameter Values in the Abstraction Model–For the abstraction model, the active-fracture model _ parameter is tabulated for the lower-bound, mean, and upper-bound infiltration scenarios for the model layers in Tables C-2 to C-4 (BSC 2004 [DIRS 162730], Tables 6-8 to 6-10). A constant fracture residual saturation of 0.01 is used for all layers.

Table C-2. Fracture _ Parameter for Lower-Bound Infiltration Scenario

Rock Layer	Fracture _	Rock Layer	Fracture _	Input Description	Type of Uncertainty
tcwf1	0.4834	ch1fz	0.2759	This value is read in by FEHM and used in calculating fracture spacing values based on the active-fracture model.	Fixed value for each layer but varies from layer to layer. The value also depends on climate.
tcwf2	0.4834	ch2fz	0.2759		
tcwf3	0.4834	ch3fz	0.2759		
ptnf1	0.1032×10^{-1}	ch4fz	0.2759		
ptnf2	0.1032×10^{-1}	ch5fz	0.2759		
ptnf3	0.1032×10^{-1}	ch6fz	0.2759		
ptnf4	0.1032×10^{-1}	pp4fz	0.2759		
ptnf5	0.1032×10^{-1}	pp3fd	0.2476		
ptnf6	0.1032×10^{-1}	pp2fd	0.2476		
tswf1	0.3741×10^{-1}	Pp1fz	0.2776		
tswf2	0.5284	bf3fd	0.2476		
tswf3	0.5284	bf2fz	0.2759		
tswf4	0.4764	tr3fd	0.2476		
tswf5	0.4764	tr2fz	0.2759		
tswf6	0.4764	pcf38	0.00		
tswf7	0.4764	pcf39	0.00		
tswf8	0.4764	Pc1fz	0.00		
tswfz	0.2759	Pc2fz	0.00		
tswfv	0.2500	Pc5fz	0.00		
ch1fv	0.2500	Pc6fz	0.00		
ch2fv	0.2500	pc4fp	0.00		
ch3fv	0.2500	tcwff (fault)	0.4000		
ch4fv	0.2500	ptnff (fault)	0.1138		
ch5fv	0.2500	tswff (fault)	0.3000		
ch6fv	0.2500	chnff (fault)	0.3000		

Source: BSC 2004 [DIRS 162730], Table 6-8.

Table C-3. Fracture _ Parameter for Mean Infiltration Scenario

Rock Layer	Fracture _	Rock Layer	Fracture _	Input Description	Type of Uncertainty
tcwf1	0.5866	ch1fz	0.3704	This value is read in by FEHM and used in calculating fracture spacing values based on the active-fracture model.	Fixed value for each layer but varies from layer to layer. The values also depend on climate.
tcwf2	0.5866	ch2fz	0.3704		
tcwf3	0.5866	ch3fz	0.3704		
ptnf1	0.9051×10^{-1}	ch4fz	0.3704		
ptnf2	0.9051×10^{-1}	ch5fz	0.3704		
ptnf3	0.9051×10^{-1}	ch6fz	0.3704		
ptnf4	0.9051×10^{-1}	pp4fz	0.3704		
ptnf5	0.9051×10^{-1}	pp3fd	0.1989		
ptnf6	0.9051×10^{-1}	pp2fd	0.1989		
tswf1	0.1289	pp1fz	0.3704		
tswf2	0.6000	bf3fd	0.1989		
tswf3	0.6000	bf2fz	0.3704		
tswf4	0.5686	tr3fd	0.1989		
tswf5	0.5686	tr2fz	0.3704		
tswf6	0.5686	pcf38	0.00		
tswf7	0.5686	pcf39	0.00		
tswf8	0.5686	pcf1z	0.00		
tswfz	0.3704	pcf2z	0.00		
tswfv	0.2500	pcf5z	0.00		
ch1fv	0.2500	pcf6z	0.00		
ch2fv	0.2500	pcf4p	0.00		
ch3fv	0.2500	tcwff (fault)	0.4000		
ch4fv	0.2500	ptnff (fault)	0.1138		
ch5fv	0.2500	tswff (fault)	0.3000		
ch6fv	0.2500	chnff (fault)	0.3000		

Source: BSC 2004 [DIRS 162730], Table 6-9.

Table C-4. Fracture _ Parameter for Upper-Bound Infiltration Scenario

Rock Layer	Fracture _	Rock Layer	Fracture _	Input Description	Type of Uncertainty
tcwf1	0.5000	ch1fz	0.5000	This value is read in by FEHM and used in calculating fracture spacing values based on the active-fracture model.	Fixed value for each layer but varies from layer to layer. The value also depends on climate.
tcwf2	0.5000	ch2fz	0.5000		
tcwf3	0.5000	ch3fz	0.5000		
ptnf1	0.8319×10^{-1}	ch4fz	0.5000		
ptnf2	0.8319×10^{-1}	ch5fz	0.5000		
ptnf3	0.8319×10^{-1}	ch6fz	0.5000		
ptnf4	0.8319×10^{-1}	pp4fz	0.5000		
ptnf5	0.8319×10^{-1}	pp3fd	0.5000		
ptnf6	0.8319×10^{-1}	pp2fd	0.5000		
tswf1	0.1000	pp1fz	0.5000		
tswf2	0.5606	bf3fd	0.5000		
tswf3	0.5606	bf2fz	0.5000		
tswf4	0.5700	tr3fd	0.5000		
tswf5	0.5700	tr2fz	0.5000		
tswf6	0.5700	pcf38	0.0000		
tswf7	0.5700	pcf39	0.0000		
tswf8	0.5700	pcf1z	0.0000		
tswfz	0.5000	pcf2z	0.0000		
tswfv	0.2500	pcf5z	0.0000		
ch1fv	0.2500	pcf6z	0.0000		
ch2fv	0.2500	pcf4p	0.0000		
ch3fv	0.2500	tcwff (fault)	0.4000		
ch4fv	0.2500	ptnff (fault)	0.1138		
ch5fv	0.2500	tswff (fault)	0.3000		
ch6fv	0.2500	chnff (fault)	0.3000		

Source: BSC 2004 [DIRS 162730], Table 6-10.

C.3.3 Adaptation of the Active-Fracture Model for Abstraction Transport Model Calculations

Particle Tracking Model and Abstraction of Transport Processes (BSC 2004 [DIRS 162730], Section III-5) describes the method for adapting the active-fracture model for abstraction transport model calculations. The active-fracture model is incorporated into the model by effectively reducing the interfacial area and the fracture frequency to account for the fact that not all fractures are flowing. Active-fracture model-based adjustments in terms of _ and S_e are applied to the interface area and fracture spacing. Aperture values are not changed. The detailed discussion is presented in Section C.4.3.

The following addresses the question of whether the fraction of active fractures is factored into the calculation of fluid velocity in the transport model. The fraction of active fractures is implicitly considered in the calculation of fluid velocity in the transport model because the flow fields are developed and imported directly into the transport abstraction model. Fluid residence time in the fractures is equal to the volume of water in a computational cell divided by the

volumetric flow rate of the fluid. In turn, the volume of fluid in a cell is the total volume times the volumetric water content. All these terms are calculated in flow model simulations and imported into the transport model. Therefore, fluid velocities and transport times do not need any further adjustment to account for active fractures because the flow field calculations have already accounted for the active-fracture concept.

C.3.4 Verification of the Active-Fracture Model with Matrix Diffusion Integration in Total System Performance Assessment Abstraction (TSPAI 3.29)

In *Particle Tracking Model and Abstraction of Transport Processes* (BSC 2004 [DIRS 162730], Section 7), the implementation of the active-fracture model in the abstraction model was shown to reproduce the qualitative features of the breakthrough curves documented in the process model reports on which the abstraction is based. Thus, the abstraction model has been compared with the full complexity of the unsaturated zone model and found to be able to represent the system robustly and efficiently for the entire range of parameters and conceptual models required. The following tests were documented in *Particle Tracking Model and Abstraction of Transport Processes* (BSC 2004 [DIRS 162730], Section 7) and are summarized below (see Section C.4.4 for additional details).

Comparison with the Dual-K and MINC Model Formulations on a Two-Dimensional Cross-Sectional Model–*Particle Tracking Model and Abstraction of Transport Processes* (BSC 2004 [DIRS 162730], Section 7.2) describes the comparison of the particle tracking model for abstraction with simulations from *Radionuclide Transport Models Under Ambient Conditions* (BSC 2003 [DIRS 163228]) using the T2R3D code (LBNL 1999 [DIRS 146654]) in a two-dimensional cross-sectional model. The particle tracking model tests two alternative conceptual models to describe fracture–matrix interactions: the discrete fracture model and the dual-k formulation. The T2R3D process model uses both the dual-k and multiple interacting continua (MINC) formulations. The conceptual model for the fracture–matrix interactions is shown to impact the predicted behavior, especially for the fastest traveling portion of the solute. Comparisons for the range of diffusion behavior also show that the abstraction model compares adequately with the process models and properly accounts for the role of conceptual model uncertainty in the fracture–matrix interaction model.

Comparison with T2R3D Process Model for Three-Dimensional System–The abstraction transport model results are compared with results from T2R3D, documented in *Radionuclide Transport Models Under Ambient Conditions* (BSC 2003 [DIRS 163228]) and summarized in Section 7.4. The agreement between these models shows that all significant features of the unsaturated zone transport system are captured with the abstraction model. The abstraction model is also shown to produce reasonable results for a wide range of diffusion coefficients. The comparison of different fracture–matrix interaction models for the FEHM particle tracking model are also reasonable and provide additional evidence for the correct functioning of the fracture–matrix interaction model. The sensitivity of breakthrough of a conservative tracer to the active-fracture model _ parameter is consistent between the two models, further verifying that the implementation of the active-fracture model with matrix diffusion in the abstraction model replicates the behavior of the process model.

The information in this report is responsive to agreements TSPAI 3.28 and 3.29 made between the DOE and the NRC. The report contains the information that the DOE considers necessary for the NRC to review for closure of this agreement.

C.4 BASIS FOR THE RESPONSE

C.4.1 Independent Lines of Evidence

C.4.1.1 Groundwater Age Predictions Compared to ^{14}C Measurements

The unsaturated zone of Yucca Mountain is a quasi-steady-state flow system, with very small infiltration and percolation rates. The matrix pore-water age corresponds to the mean time required for the groundwater to travel from the ground surface to where it is sampled in the system. The age can be considered constant at each location in this quasi-steady-state flow system, but spatially variable. The migration of water molecules is governed by advection and diffusion, similar to solute transport (Goode 1996 [DIRS 162573]). Thus, tracer transport times (ages) can be simulated using a conservative transport model.

The detailed description of the simulation of groundwater ages in the unsaturated zone and comparison with ^{14}C data can be found in *Analysis of Hydrologic Properties Data* (BSC 2003 [DIRS 161773], Section 7.2.1). ^{14}C data were collected from perched water, pore water, and gas samples from the Yucca Mountain unsaturated zone (BSC 2002 [DIRS 160247], Section 6.6.4). ^{14}C data from gas samples are considered to be most representative of in situ conditions and are interpreted to be representative of ages of the in situ pore water (Yang 2002 [DIRS 160839], Section 4.1.2). ^{14}C data from perched water are not used for active-fracture model testing because perched water comes mainly from matrix flow through the PTn, which is insensitive to the active-fracture model parameters (Wang 2003 [DIRS 161654]). ^{14}C residence ages (BSC 2002 [DIRS 160247], Table 20) were calculated using the data from two boreholes, USW SD-12 and USW UZ-1.

One-dimensional numerical models were developed for the boreholes and the rock properties were taken from calibration with present-day, mean infiltration maps. The value of the active-fracture model parameter _ for model layers within the repository horizon (tsw32 to tsw38, see Table 4-1 for the definition of model layers) is varied for different simulations as a sensitivity test. The top boundary condition corresponds to the present-day infiltration rate for flow and a constant tracer concentration for transport simulations. Simulated water transport times (or ages) for rock matrices are compared with ^{14}C ages. A simulated water transport time at a given depth (or average transport time for water particles from the ground surface) is determined as the time when the matrix concentration reaches 50 percent of the top boundary concentration.

Figure C-1 shows simulated water ages for different _ values of unsaturated zone model layers tsw32 to tsw38. The considerable sensitivity of simulated results to _ indicates that ^{14}C data are useful for validating the active-fracture model and for constraining the _ values for the TSw unit. For _ values ranging from 0.2 to 0.4, simulated results approximately match the observations. A larger _ value generally corresponds to a longer time for transport into the matrix because of a smaller degree of matrix diffusion, resulting from a smaller fracture–matrix interfacial area available for mass transport between fractures and the matrix.

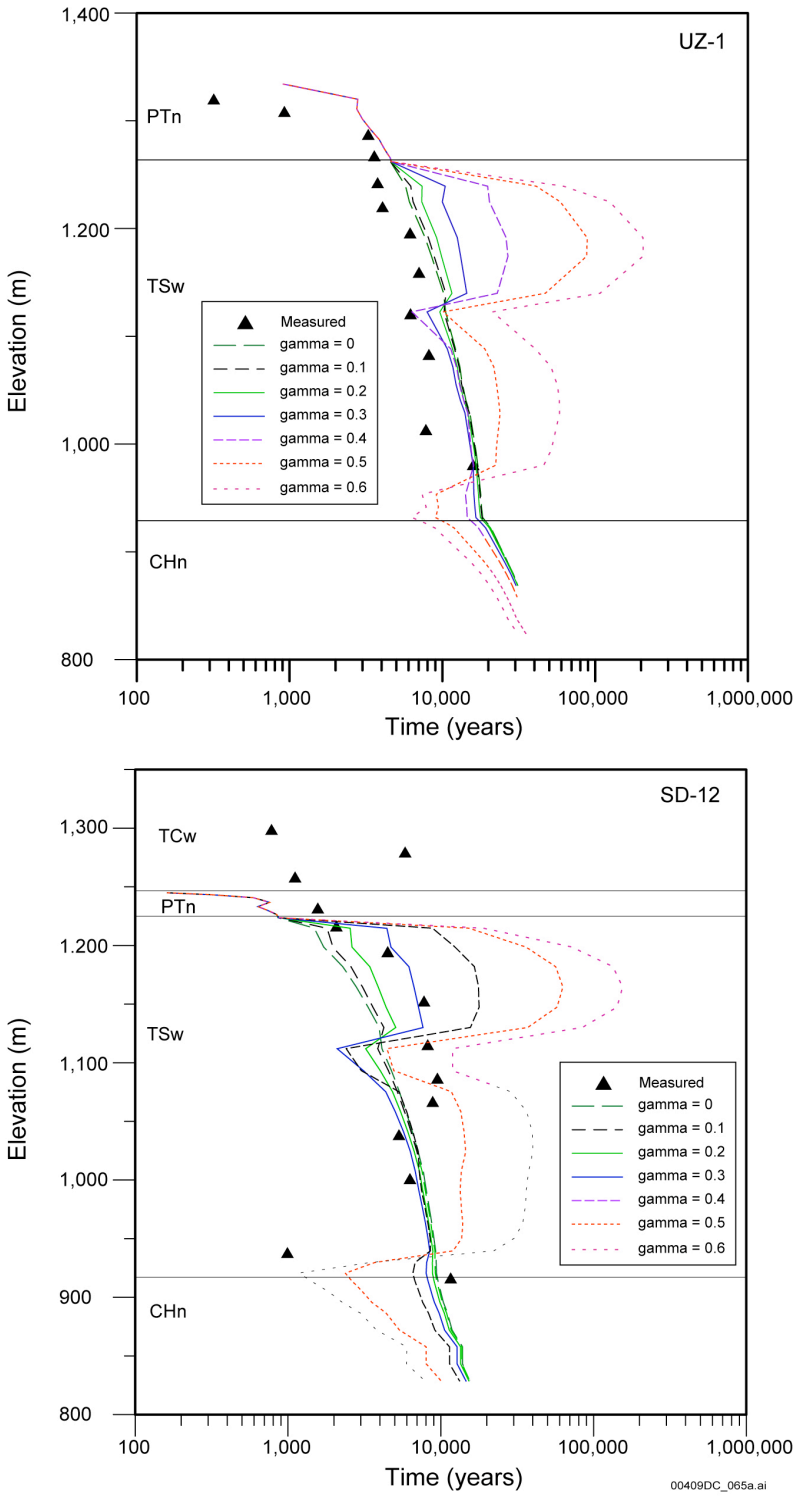

Source: BSC 2003 [DIRS 161773], Figure 13.

Figure C-1. Comparisons between One-Dimensional Simulated Water Transport Times (Ages) in the Rock Matrix at Boreholes for Several _ Values with Measured ^{14}C Ages at Boreholes USW UZ-1 and USW SD-12

Simulated water ages increase sharply at an elevation of about 1,100 m for two boreholes (Figure C-1). This is because the upper portion of the TSw unit has relatively small fracture density values and, consequently, a smaller degree of matrix diffusion for a given _ value (Table C-5). For borehole USW UZ-1, the simulated water ages are generally greater than the observations. This may be a result of larger fracture densities (and consequently more matrix diffusion) at the borehole location compared to the layer-averaged fracture properties used in the unsaturated zone model (BSC 2003 [DIRS 161773], Section 5). The results are fairly insensitive to _ values less than 0.2, and a _ value of 0.2 to 0.4 best captures the magnitude and trends of the measured data in both boreholes.

Table C-5. Fracture Properties for Unsaturated Zone Model Layers

UZ Model Layer	Permeability (m^2)				Frequency (m^{-1})			Van Genuchten parameter			porosity (-)	Std (-)	Afm
	k_G	$\log(k_G)$	$\sigma_{\log(kG)}$	N	f	σ_f	N	α (Pa^{-1})	$\log(\alpha)$	m (-)			
tcw11	3.0×10^{-11}	-10.52	-	2	0.92	0.94	76	5.0×10^{-3}	-2.30	0.633	2.4×10^{-2}	-	1.56
tcw12	5.3×10^{-12}	-11.28	0.78	80	1.91	2.09	1241	2.2×10^{-3}	-2.66	0.633	1.7×10^{-2}	-	13.39
tcw13	4.5×10^{-12}	-11.35	1.15	3	2.79	1.43	60	1.9×10^{-3}	-2.73	0.633	1.3×10^{-2}	-	3.77
ptn21	3.2×10^{-12}	-11.49	0.88	12	0.67	0.92	76	2.7×10^{-3}	-2.57	0.633	9.2×10^{-3}	-	1
ptn22	3.0×10^{-13}	-12.52	0.20	4	0.46	-	-	1.4×10^{-3}	-2.86	0.633	1.0×10^{-2}	-	1.41
ptn23	3.0×10^{-13}	-12.52	0.20	4	0.57	-	63	1.2×10^{-3}	-2.91	0.633	2.1×10^{-3}	-	1.75
ptn24	3.0×10^{-12}	-11.52	-	1	0.46	0.45	18	3.0×10^{-3}	-2.53	0.633	1.0×10^{-2}	-	0.34
ptn25	1.7×10^{-13}	-12.78	0.10	7	0.52	0.6	72	1.1×10^{-3}	-2.96	0.633	5.5×10^{-3}	-	1.09
ptn26	2.2×10^{-13}	-12.66	-	1	0.97	0.84	114	9.6×10^{-4}	-3.02	0.633	3.1×10^{-3}	-	3.56
tsw31	8.1×10^{-13}	-12.09	-	-	2.17	2.37	140	1.1×10^{-3}	-2.96	0.633	5.0×10^{-3}	-	3.86
tsw32	7.1×10^{-13}	-12.15	0.66	31	1.12	1.09	842	1.4×10^{-3}	-2.86	0.633	8.3×10^{-3}	-	3.21
tsw33	7.8×10^{-13}	-12.11	0.61	27	0.81	1.03	1329	1.6×10^{-3}	-2.80	0.633	5.8×10^{-3}	-	4.44
tsw34	3.3×10^{-13}	-12.48	0.47	180	4.32	3.42	10646	6.7×10^{-4}	-3.18	0.633	8.5×10^{-3}	2.50×10^{-3}	13.54
alternate tsw34	1.5×10^{-13}	-12.81	0.75	180									
tsw35	9.1×10^{-13}	-12.04	0.54	31	3.16	-	595	1.0×10^{-3}	-2.99	0.633	9.6×10^{-3}	-	9.68
tsw3[67]	1.3×10^{-12}	-11.87	0.28	19	4.02	-	526	1.1×10^{-3}	-2.96	0.633	1.3×10^{-2}	-	12.31
tsw38	8.1×10^{-13}	-12.09	-	-	4.36	-	37	8.9×10^{-4}	-3.05	0.633	1.1×10^{-2}	-	13.34
tsw39	8.1×10^{-13}	-12.09	-	-	0.96	-	46	1.5×10^{-3}	-2.82	0.633	4.3×10^{-3}	-	2.95
ch1Ze	2.5×10^{-14}	-13.60	-	-	0.04	-	3	1.4×10^{-3}	-2.86	0.633	1.6×10^{-4}	-	0.11
ch1VI	2.2×10^{-13}	-12.66	-	-	0.10	-	11	2.1×10^{-3}	-2.69	0.633	6.1×10^{-4}	-	0.3
ch[23456]VI	2.2×10^{-13}	-12.66	-	-	0.14	-	25	1.9×10^{-3}	-2.73	0.633	7.7×10^{-4}	-	0.43
ch[2345]Ze	2.5×10^{-14}	-13.60	-	1	0.14	-	25	8.9×10^{-4}	-3.05	0.633	3.7×10^{-4}	-	0.43
ch6	2.5×10^{-14}	-13.60	-	-	0.04	-	-	1.4×10^{-3}	-2.86	0.633	1.6×10^{-4}	-	0.11
pp4	2.5×10^{-14}	-13.60	-	-	0.14	-	-	8.9×10^{-4}	-3.05	0.633	3.7×10^{-4}	-	0.43
pp3	2.2×10^{-13}	-12.66	-	-	0.20	-	-	1.6×10^{-3}	-2.78	0.633	9.7×10^{-4}	-	0.61
pp2	2.2×10^{-13}	-12.66	-	-	0.20	-	-	1.6×10^{-3}	-2.78	0.633	9.7×10^{-4}	-	0.61
pp1	2.5×10^{-14}	-13.60	-	-	0.14	-	-	8.9×10^{-4}	-3.05	0.633	3.7×10^{-4}	-	0.43
bf3	2.2×10^{-13}	-12.66	-	-	0.20	-	-	1.6×10^{-3}	-2.78	0.633	9.7×10^{-4}	-	0.61
bf2	2.5×10^{-14}	-13.60	-	-	0.14	-	-	8.9×10^{-4}	-3.05	0.633	3.7×10^{-4}	-	0.43
tr3	2.2×10^{-13}	-12.66	-	-	0.20	-	-	1.6×10^{-3}	-2.78	0.633	9.7×10^{-4}	-	0.61
tr2	2.5×10^{-14}	-13.60	-	-	0.14	-	-	8.9×10^{-4}	-3.05	0.633	3.7×10^{-4}	-	0.43

Source: BSC 2003 [DIRS 161773], Table 7.

NOTE: k is permeability (geometric mean).
σ is standard deviation.
N is number of samples.
f is fracture frequency.
α and m are fitting parameters for the van Genuchten water potential relationship.
Std refers to standard deviation for fracture porosity.
Afm refers to fracture–matrix interface area (m^2/m^3).
"-" means that no data are available.

Estimating groundwater age in the unsaturated zone was also tested with a three-dimensional tracer transport model based on the calibrated groundwater flow field (BSC 2003 [DIRS 163045], Section 7.5). The three-dimensional transport model simulation was performed using T2R3D V1.4 (LBNL 1999 [DIRS 146654]). The three-dimensional flow field obtained with the base-case water-flow simulation (present-day, mean infiltration) is incorporated to simulate the matrix pore-water age in the entire model domain. A pulse tracer source is introduced on the ground surface through fractures, and the tracer concentration in rock matrix in the entire domain was observed. The simulated matrix pore-water age, at a specific location, is then identified as the time required for the tracer pulse (appearing as concentration peaks in the unsaturated zone) to travel to that location and is determined from the concentration breakthrough curve.

The simulated matrix pore-water ages for boreholes UZ-1 and SD-12 were plotted and compared to the measured age data (^{14}C) used for the one-dimensional study (Figures C-2 and C-3). These figures show that the simulated matrix pore-water ages in the upper portion of the TSw unit are larger than the measured ^{14}C ages for a _ value of 0.6. This is caused mainly by the underestimated advective and diffusive solute flux between fractures and matrix along these subunits. The smaller the flux or the slower the diffusion from fractures to matrix, the older the ages for matrix pore water, which occurs for larger _ values.

Figure C-2 (UZ-1) shows that the simulated matrix pore-water ages for the upper TSw units with a _ value of 0.4 match the measured ^{14}C ages well. Simulated ages for lower TSw units are a little bit younger than the measurements but are also within the range of measured ^{14}C age of TSw units. Figure C-3 (SD-12) shows that the match between the simulated groundwater ages using a _ value of 0.4 and the measurements is reasonably close (the simulated ages for TSw unit are within the range of the measured ^{14}C age of TSw units).

The larger _ (0.6 for the TSw units) used in the base-case unsaturated zone flow model gives slightly earlier breakthrough times for solute transport from the repository to the water table and, therefore, provides more conservative results. This is because a larger _ factor corresponds to a larger fracture pore velocity and a smaller effective fracture–matrix interface area (or a smaller degree of fracture–matrix interaction) (BSC 2003 [DIRS 163045], Section 6.8).

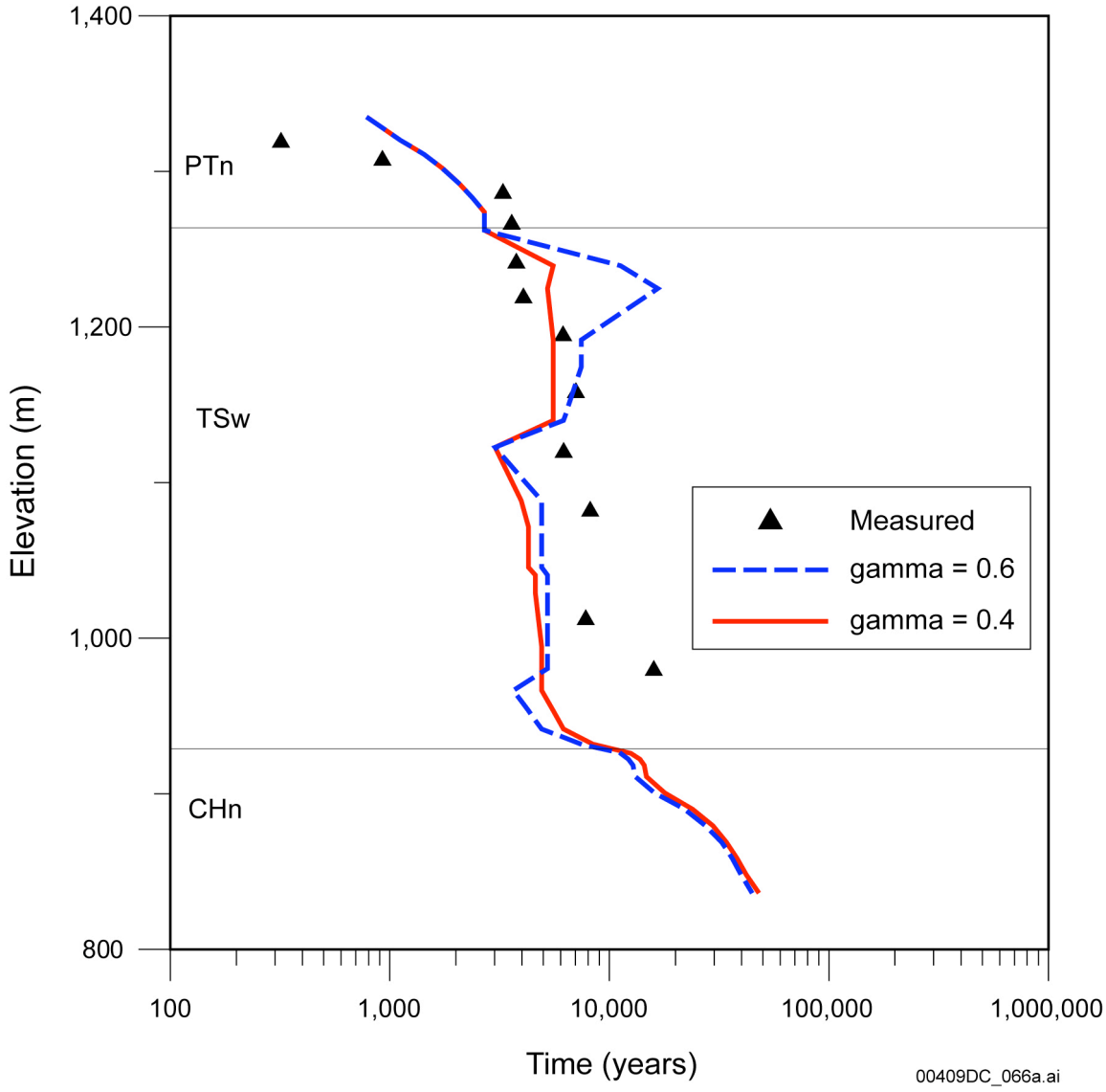

Source: BSC 2003 [DIRS 163045], Figure 7.5-1.

Figure C-2. Simulated Groundwater Age for Borehole UZ-1 Compared to the Measured ^{14}C Age

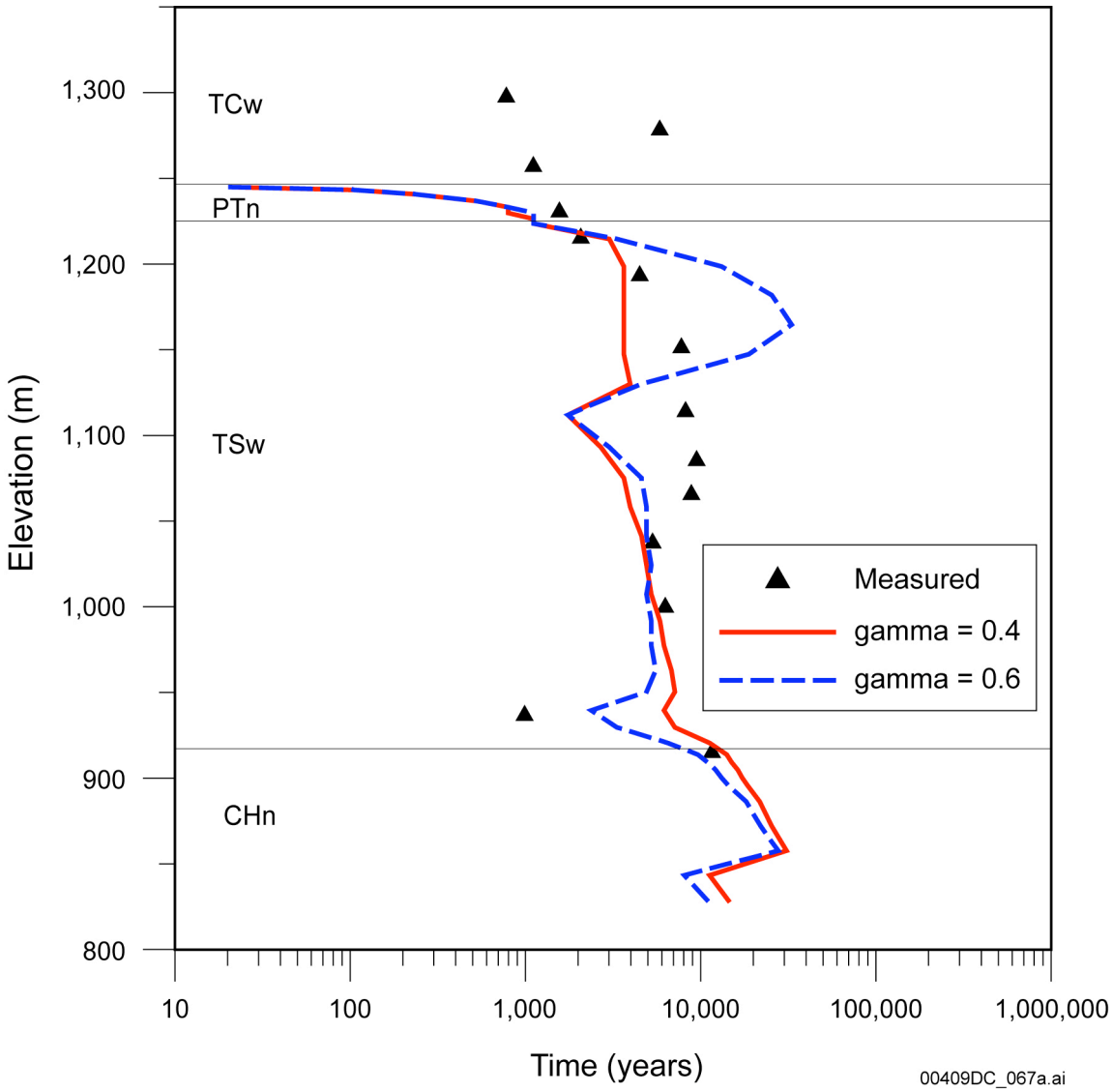

Source: BSC 2003 [DIRS 163045], Figure 7.5-2.

Figure C-3. Simulated Groundwater Age for Borehole SD-12 Compared to the Measured ^{14}C Age

C.4.1.2 Simulation of Fraction of Active Fractures Compared to Mineral Fracture Coating Data

Fracture coating is generally a signature of water flow paths. Therefore, the coating data are useful for testing the active-fracture model that describes water flow in fractures. Details of this effort can be found in *Analysis of Hydrologic Properties Data* (BSC 2003 [DIRS 161773], Section 7.2.2).

The observed spatial distribution in the ESF of fractures with coatings is used to estimate the portion of active fractures in the unsaturated zone. For a given survey interval along the ESF, a frequency of coated fractures can be estimated for a geologic unit, based on the total number of coated fractures. The ratio of coated-fracture frequency to total fracture frequency provides an

estimate of the portion of active fracture for the given geologic unit (Wang 2003 [DIRS 161654]). The estimated average portion of the active fracture for the TSw is 7.2 percent.

The abundance of mineral coating (coating volume divided by total rock volume), divided by the corresponding fracture porosity, gives another estimate of the portion of the active fractures in the unsaturated zone under ambient conditions. Abundance data for all intervals in welded tuffs have an arithmetic mean of 0.084 percent (BSC 2002 [DIRS 160247], Section 6.10.1.1), while a typical fracture porosity is 1 percent (Table C-5). Therefore, an estimate of the average portion of active fractures for welded units is 8.4 percent, close to the estimate determined from the frequency of coated fractures. While fracture coatings may not precisely represent active flow paths in the unsaturated zone and some flow paths may not have coatings (Liu et al. 1998 [DIRS 105729]), these values at least give a rough estimate of lower limits for the portion of active fractures in the unsaturated zone (about 10 percent).

Mineral growth rate data imply that the unsaturated zone fracture network has maintained a large degree of hydrologic stability over time and that fracture flow paths in the deep unsaturated zone are buffered from climate-induced variations in precipitation and infiltration (BSC 2002 [DIRS 160247], Section 6.10.3.9). If the active-fracture model actually represents water flow processes in the unsaturated zone, modeling results based on the active-fracture model should be consistent with this important observation.

To check the consistency of the active-fracture model against the coating data, a one-dimensional model for borehole USW SD-12 is used. The model is the same as that used for the one-dimensional ^{14}C simulations and described in *Analysis of Hydrologic Properties Data* (BSC 2003 [DIRS 161773], Section 7.2.1) and in Section C.4.1.1. USW SD-12 is chosen because it is located near the middle of the ESF, where coating data were collected. Two infiltration rates, present-day mean infiltration rate and glacial maximum infiltration rate, are used for simulations. The latter infiltration rate is about five times as large as the former rate and represents the maximum infiltration rate in past climates. Uniform _ distributions within model layers tsw32 to tsw38 are employed.

Figure C-4 shows the simulated average portion of active fractures, f_a, for the relevant model layers (tsw32 to tsw38) as a function of infiltration rate and _. The average portion is calculated from $f_a = S_e^{\gamma}$ using the average effective saturation S_e for model layers tsw32 to tsw38. The calculated f_a values range about 10 percent for _ values close to 0.4, which are similar to those used for matching the ^{14}C data. For the same range of _ values, the calculated f_a values do not change significantly for the two infiltration rates (Figure C-4), which is consistent with the observation of flow-path stability over time.

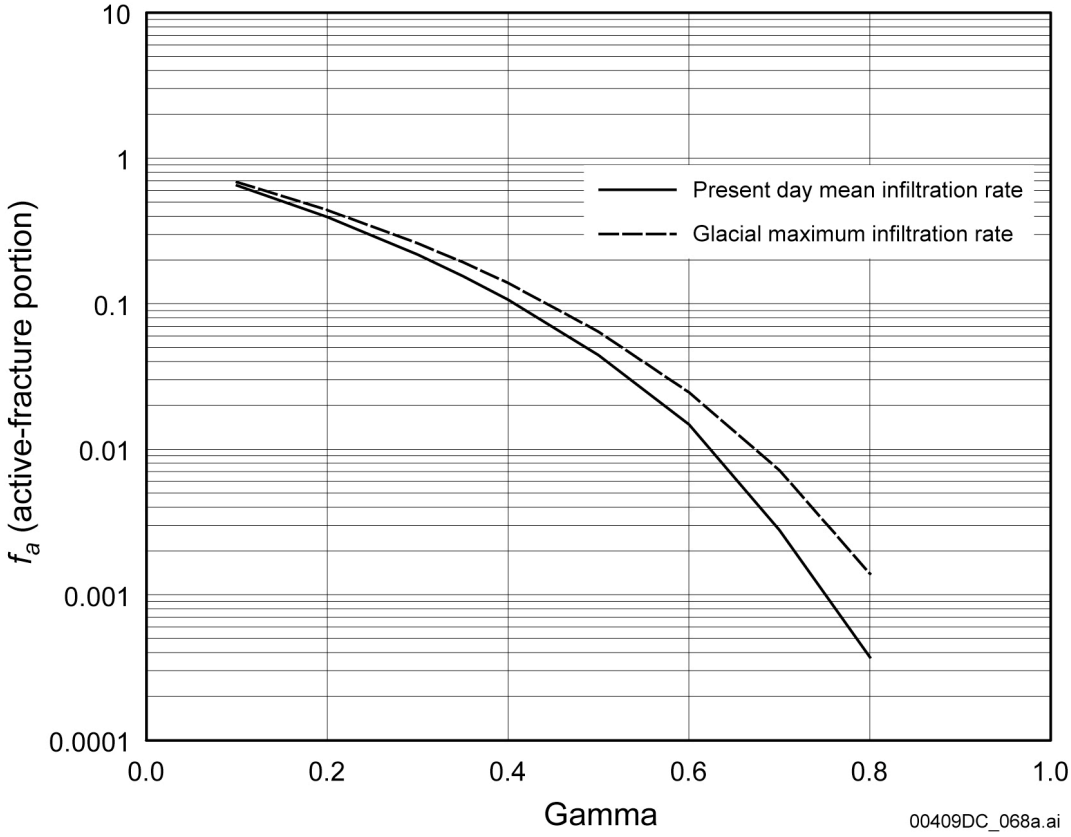

Source: BSC 2003 [DIRS 161773], Figure 14.

Figure C-4. Simulated Average Portion of Active Fracture for the Relevant Model Layers (tsw32 to tsw38) as a Function of Infiltration Rate and _

In summary, the simulation results based on the active-fracture model are consistent with both ^{14}C data and fracture coating data for a similar range of _ values.

C.4.1.3 Consistency between Active-Fracture Model and Fractal Flow Patterns

Unsaturated flow patterns in a fracture network are expected to be (at least approximately) fractal. This is supported by fracture coating data from the unsaturated zone of Yucca Mountain and an analysis from *Analysis of Hydrologic Properties Data* (BSC 2003 [DIRS 161773], Section 6.7) showing that the distribution of coated fractures in the ESF are consistent with a fractal model. Detailed line survey data for coated fractures from the Tptpmn (tsw34) unit (which has the largest number of survey intervals) are analyzed using the box counting method.

In *Analysis of Hydrologic Properties Data* (BSC 2003 [DIRS 161773], Section 6.7), a correspondence between _ and the fractal dimension of the flow system is also derived and shows that the active-fracture model can simulate fractal flow behavior in an unsaturated fracture network. This correspondence improves confidence in the active-fracture model because it demonstrates that it is theoretically consistent with an independently derived fractal conceptualization of unsaturated flow that is supported by field data. This section presents the analysis of the fracture coating data and derivation of the correspondence between _ and the

fractal dimension of the flow system from *Analysis of Hydrologic Properties Data* (BSC 2003 [DIRS 161773], Section 6.7).

The locations of the coated fractures along the survey line form a set of points in a one-dimensional space. For a given box size (length of a segment) l, there are $30/l$ small boxes (or segments) for a given survey interval that is 30 m long. N in this section denotes total numbers of boxes that cover at least one location of the coated fractures (along the survey line) for all the survey intervals. Figure C-5 shows that the observed N values as a function of l can be fitted by a power function with a power of _0.5 that corresponds to a fractal dimension of 0.5 for the set of points. This indicates that coated fractures may result from a fractal flow pattern in the corresponding fracture network.

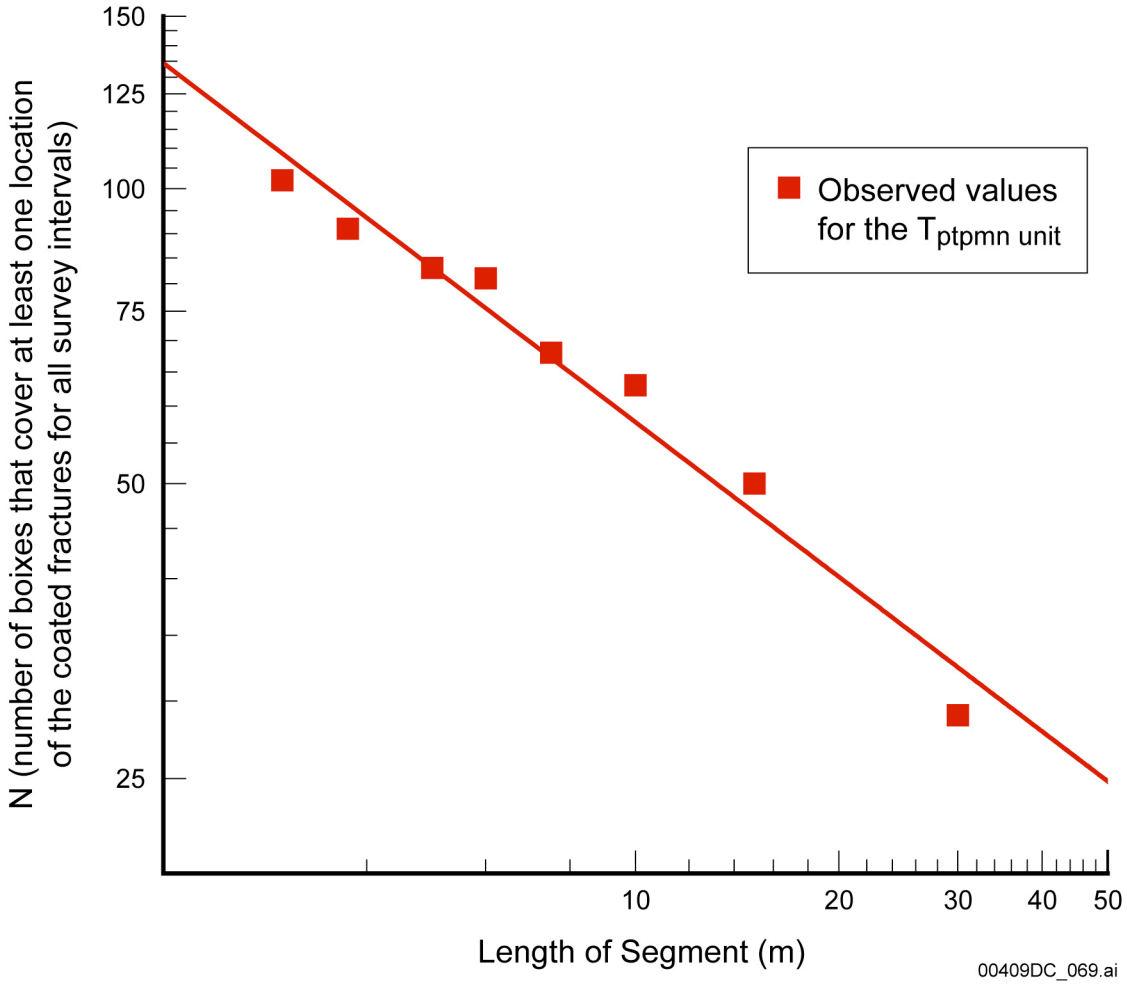

Source: BSC 2003 [DIRS 161773], Figure 7.

NOTE: The data points correspond to observed values for the Tptpmn unit.

Figure C-5. Relation between N and l

A fractal pattern is characterized by the fractal dimension, d_f, that is generally noninteger and less than the corresponding Euclidean dimension of a space, D. The most straightforward

method of determining d_f is based on box counting. In this case, the fractal dimension is determined from the following equation by counting the number (N) of boxes (e.g., square and cubic for two-dimensional and three-dimensional problems, respectively), needed to cover a spatial pattern, as a function of the box size (l) (Feder 1988 [DIRS 160844], pp. 14 to 15):

$$N(l) = \left(\frac{L}{l}\right)^{df} \quad \text{(Eq. C-1)}$$

(BSC 2003 [DIRS 161773], Equation 61) where L refers to the size of the whole spatial domain under consideration. Figure C-6 shows a box-counting procedure for a spatial pattern with a d_f value of 1.6 in a two-dimensional domain with size L (Yamamoto et al. 1993 [DIRS 160843], Figure 3).

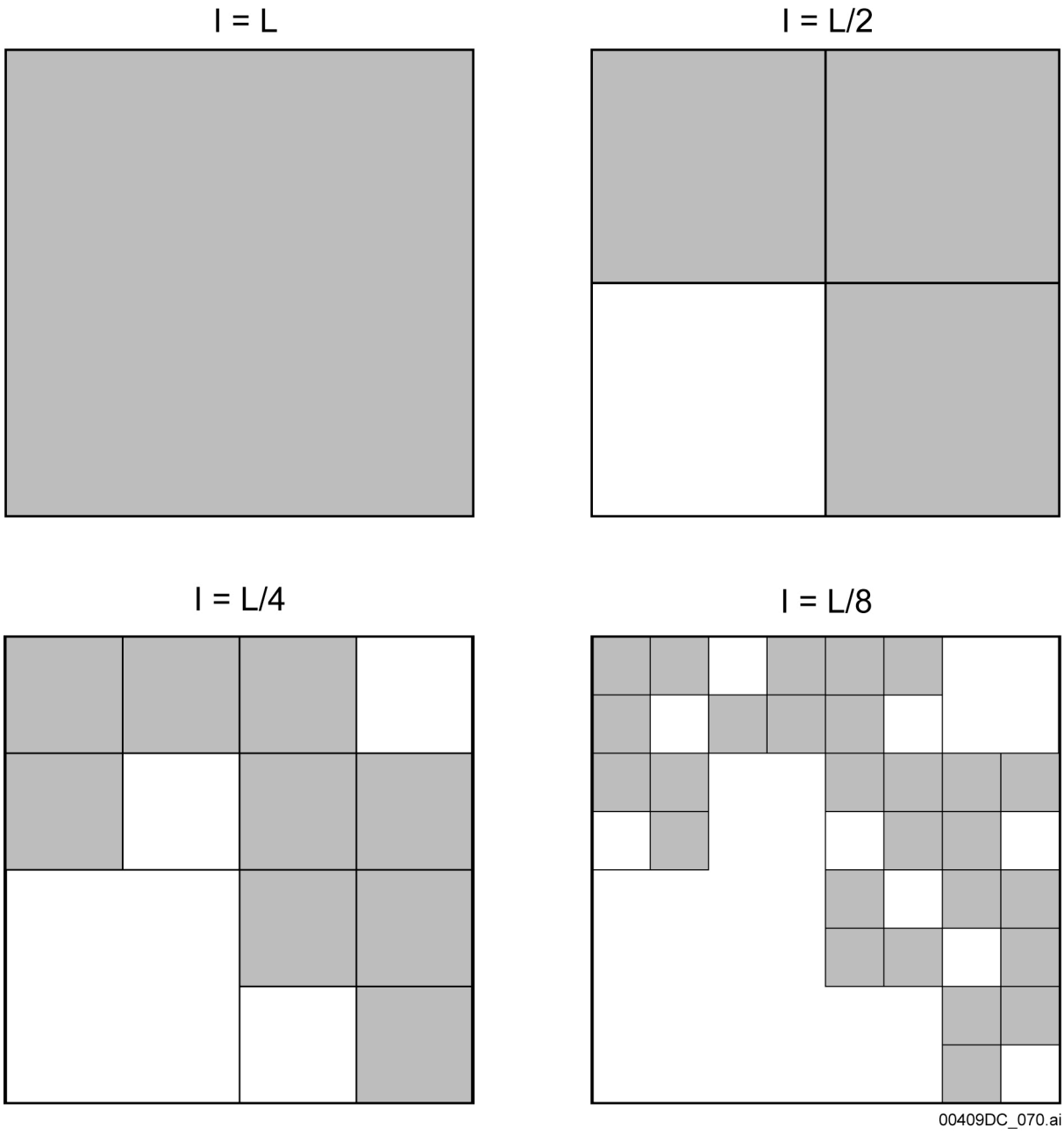

Source: BSC 2003 [DIRS 161773], Figure 8.

NOTE: Shaded areas contain saturation and active flow.

Figure C-6. Demonstration of Box Counting Procedure for Several Box Sizes

Obviously, if a spatial pattern is uniformly distributed in space, the fractal dimension will be identical to the corresponding Euclidean dimension. In this case, the box number, N^*, and the box size l have the following relation (BSC 2003 [DIRS 161773], Equation 62):

$$N^*(l) = \left(\frac{L}{l}\right)^D \quad \text{(Eq. C-2)}$$

Consider Figure C-6 to be a gridblock containing a fracture network and the corresponding flow pattern in the fracture network to be fractal. In this case, only a portion of the medium within a gridblock contributes to water flow (Figure C-6). This is conceptually consistent with the active-fracture model (Liu et al. 1998 [DIRS 105729]). In Figure C-6, a box is shaded if it covers one or more fractures (or fracture segments) that conduct water. For simplicity, fractures are assumed to be randomly distributed in space, and, thus, the dimension for water saturation distribution is the corresponding Euclidean dimension when all the connected fractures actively conduct water. Combining Equations C-1 and C-2 gives (BSC 2003 [DIRS 161773], Equation 63):

$$[N(l)]^{1/d_f} = [N^*(l)]^{1/D} \quad \text{(Eq. C-3)}$$

The average water saturation (S) for the whole gridblock (Figure C-6) is determined as (BSC 2003 [DIRS 161773], Equation 64):

$$S = \frac{V}{l^D \phi N^*(l)} \quad \text{(Eq. C-4)}$$

where V is the total water volume (excluding residual water) in fractures within the gridblock (Figure C-6), and ϕ is fracture porosity. Similarly, the average water saturation, S_b, for shaded boxes with a size of l is given as (BSC 2003 [DIRS 161773], Equation 65):

$$S_b = \frac{V}{l^D \phi N(l)} \quad \text{(Eq. C-5)}$$

From Figure C-6 (BSC 2003 [DIRS 161773], Equation 66):

$$\frac{V}{l_1^D \phi} = 1 \quad \text{(Eq. C-6)}$$

Based on Equations C-3 through C-6, the average saturation for shaded boxes with a size of l_1, S_{b1}, can be expressed by (BSC 2003 [DIRS 161773], Equation 67):

$$S_{b1} = S^{\frac{d_f}{D}} \quad \text{(Eq. C-7)}$$

Because a fractal is similar at different scales, the procedure for deriving Equation C-7 from a gridblock with size L can be applied to shaded boxes with a smaller size l_1. In this case, for a given box size smaller than l_1, the number of shaded boxes will be an averaged number for those within the relatively large shaded boxes with a size of l_1. Again, a box size $l_2 < l_1$ gives a saturation relation (BSC 2003 [DIRS 161773], Equation 68):

$$S_{b2} = (S_{b1})^{\frac{d_f}{D}} = S^{\left(\frac{d_f}{D}\right)^2} \qquad \text{(Eq. C-8)}$$

The procedure to obtain Equation C-8 can be continued until it reaches an iteration level n^* at which all the shaded boxes with a size of l_n cover active fractures only. The resultant average saturation for these shaded boxes is (BSC 2003 [DIRS 161773], Equation 69):

$$S_{bn} = (S)^{\left(\frac{d_f}{D}\right)^{n^*}} \qquad \text{(Eq. C-9)}$$

By active fracture definition, S_{bn} should be equivalent to the effective saturation of active fractures. Equation C-9 is similar to $f_a = S_e^{\gamma}$, obtained from a key hypothesis of the active-fracture model that the fraction of active fractures in an unsaturated fracture network is a power function of the average effective saturation of the network. Comparing these two equations yields (BSC 2003 [DIRS 161773], Equation 70):

$$\gamma = 1 - \left(\frac{d_f}{D}\right)^{n^*} \qquad \text{(Eq. C-10)}$$

Equation C-10 provides the first theoretical relation between the parameter _ and the fractal dimension for a fractal flow system, while _ was initially developed as an empirical parameter (Liu et al. 1998 [DIRS 105729]). Therefore, the active-fracture model essentially captures fractional flow behavior at the subgridblock scale (d_f less than D), whereas traditional continuum approaches assume a uniform flow pattern (or effective-saturation distribution) at that scale (corresponding to a d_f value of D or a _ value of 0). In other words, the active-fracture model can be used for simulating fractal flow behavior in an unsaturated fracture network that cannot be handled by the traditional continuum approach.

Equation C-10 implies that in the fractal flow model _ is not a constant, but a function of saturation, because both iteration level n^* and d_f may be dependent on water saturation for a given fracture network. However, a constant _ is a reasonable treatment at least for a limited range of water saturations (or flow conditions), which is the case for the Yucca Mountain unsaturated zone where fracture saturation is typically less than 10 percent under ambient conditions. It is not clear how _ depends on the other hydraulic parameters for a large range of water saturations. Experimental evidence seems to indicate that _ is a weak function of saturation (at least for porous media), which is discussed below. The fractal flow concept and Equation C-10) can be applied to porous media also, as long as their fingering flow patterns are

fractals. Therefore, results from porous media can be used to conceptually evaluate the relation between _ and water saturation for unsaturated fracture networks.

Based on experimental laboratory observations collected by applying water at the top of the corresponding porous media, Wang et al. (1998 [DIRS 155770], pp. 2,188 to 2,189) reported a relation between flow conditions and a parameter, F, defined as the ratio of horizontal cross-sectional area occupied by fingers to the total cross-sectional area. F corresponds to f_a, defined as the portion of active fractures in a fracture network (Liu et al. 1998 [DIRS 105729]). Wang et al. (1998 [DIRS 155770], pp. 2,188 to 2189) related F to the ratio of average water flux through the whole cross-sectional area, q, to saturated hydraulic conductivity of the porous medium, K_s, by

$$F \approx \left(\frac{q}{K_s} \right)^{1/2} \qquad \text{(Eq. C-11)}$$

for q/K_s values between 0.4 and 1.0 (BSC 2003 [DIRS 161773], Equation 71). By definition, the average water flux within fingers, q_F, can be related to q by (BSC 2003 [DIRS 161773], Equation 72):

$$q_F = \frac{q}{F} \qquad \text{(Eq. C-12)}$$

and the average water saturation of fingers, S_F, can be related to the average water saturation for the whole cross-sectional area, S_e, by (BSC 2003 [DIRS 161773], Equation 73):

$$S_F = \frac{S_e}{F} \qquad \text{(Eq. C-13)}$$

It is expected that flow within a gravitational finger is gravity dominated. In this case (BSC 2003 [DIRS 161773], Equation 74):

$$\frac{q_F}{K_s} = k_r = S_F{}^{\beta *} \qquad \text{(Eq. C-14)}$$

Equation C-14 uses the Brooks–Corey (Brooks and Corey 1964 [DIRS 156915]) model for describing relative permeability (k_r)–saturation relationship. $\beta *$ is a constant. Combining Equations C-11 to C-14 yields (BSC 2003 [DIRS 161773], Equation 75):

$$F = (S_e)^{\frac{\beta *}{1+\beta *}} \qquad \text{(Eq. C-15)}$$

Comparing the above equation with Equation 1 of Liu et al. (1998 [DIRS 105729]) gives

$$\gamma = \frac{\beta *}{1+\beta *} \qquad \text{(Eq. C-16)}$$

(BSC 2003 [DIRS 161773], Equation 76). Therefore, _ is a constant under certain conditions in porous media. Consequently, it is expected that _ should be a weak function of saturation for unsaturated fracture networks if fingering flow patterns in a porous medium are considered to be an analog of flow patterns in the networks.

Note that Equation C-16 cannot be directly used for estimating _ values for fracture networks (in the active-fracture model) because detailed flow mechanisms are different for unsaturated fractured rock and porous media. It also needs to be emphasized that Equation C-16 is valid for porous media under a condition of q/K_s equal to 0.4 to 1.0 (Wang et al. 1998 [DIRS 155770], pp. 2,188 to 2,189). The relationship between _ and other hydraulic properties has not been established for a fracture network.

C.4.2 Methods of Model Parameter Estimation and Numerical Implementation

C.4.2.1 Input Parameters for Rock Properties for the Abstraction Model

Rock properties (i.e., rock density, fracture porosity, spacing, aperture, active-fracture model parameter _, and fracture residual saturation) are used as inputs to the FEHM unsaturated zone transport model (BSC 2004 [DIRS 162730], Section 4). The validity and uncertainty of those parameters are documented in the corresponding reports *Analysis of Hydrologic Properties Data* (BSC 2003 [DIRS 161773]), *Calibrated Properties Model* (BSC 2003 [DIRS 160240]), and *UZ Flow Models and Submodels* (BSC 2003 [DIRS 163045]). In *Particle Tracking Model and Abstraction of Transport Processes* (BSC 2004 [DIRS 162730]), the mean values of those parameters are used to demonstrate the abstraction of the unsaturated zone transport model. The influence of parameter uncertainty on system performance will be studied in TSPA multiple realization runs.

C.4.2.2 Porosity Measurements

The estimation of fracture porosity is described in *Analysis of Hydrologic Properties Data* (BSC 2003 [DIRS 161773], Section 6.1.3).

C.4.2.2.1 General Strategy

Fracture porosity is herein defined as the effective porosity of fractures in which fluid flow and solute transport take place. In this study, a combination of porosity data derived from gas tracer tests in the ESF and porosity estimates based on the geometry of fracture networks are used to develop representative fracture porosities for the unsaturated zone model layers.

Gas tracer tests were performed in the ESF to obtain estimates of the effective fracture porosity for the Topopah Spring middle nonlithophysal welded tuff, corresponding to the tsw34 model layer. Since gas tracer transport times through the fractured rocks are directly related to the storage of the corresponding fracture networks, analyses of tracer breakthrough data can provide reliable estimates of fracture porosity for the model layer tsw34.

Gas tracer test data are available only for model layer tsw34. Fracture porosity in the other model layers is estimated from equations relating the geometry of fracturing observed in the ESF

which are normalized by the values derived from the gas tracer tests for tsw34 according to *Analysis of Hydrologic Properties Data* (BSC 2003 [DIRS 161773], Equation 12):

$$\phi_{\text{model layer x}} = \phi_{tsw34} \frac{\phi_{\text{2-D, model layer x}}}{\phi_{\text{2-D, tsw34}}} \quad \text{or} \quad \phi_{\text{model layer x}} = \phi_{tsw34} \frac{\phi_{\text{1-D, model layer x}}}{\phi_{\text{1-D, tsw34}}} \qquad \text{(Eq. C-17)}$$

where7 ϕ_{tsw34} is fracture porosity for tsw34, estimated from the gas tracer data, and $\phi_{1\text{-}D}$ and $\phi_{2\text{-}D}$ are the one-dimensional and two-dimensional porosities determined from one-dimensional borehole and two-dimensional mapping data, respectively. A so-called two-dimensional porosity for a model layer can be estimated using the aperture and the total fracture length per unit area (fracture intensity). The fracture intensity is based on tracer lengths given by the detailed line survey in the ESF and the area enclosing the traces (see Equation C-27, Section C.4.2.3). The equation used to calculate the two-dimensional porosity (BSC 2003 [DIRS 161773], Equation 10) is:

$$\phi_{2-D} = bI \qquad \text{(Eq. C-18)}$$

where b is the fracture aperture, and I is the fracture intensity (m/m^2). When no intensity data are available (in cases where the unit does not intersect any portion of the ESF or Enhanced Characterization of the Repository Block (ECRB) Cross-Drift) (BSC 2001 [DIRS 159725], Section 6.1), the one-dimensional porosity can be estimated by treating all fractures as continuous. The one-dimensional porosity is then calculated by (BSC 2003 [DIRS 161773], Equation 11):

$$\phi_{1-D} = b\overline{f} \qquad \text{(Eq. C-19)}$$

where $\overline{f}$ is the mean fracture frequency.

A large degree of uncertainty exists in the estimates based on Equations C-18 and C-19 for the following reasons. First, the estimated apertures are hydraulic apertures and may be very different from the average geometric apertures, since they are estimated based on air-permeability data. Second, Equations C-18 and C-19 only consider two-dimensional or one-dimensional geometric features, while actual fracture networks are three-dimensional. However, the use of Equation C-17 reduces this uncertainty by normalizing these relationships by the more reliable gas-tracer estimates in tsw34.

The developed fracture porosity values for the unsaturated zone model layers are given in Table C-5. All of these values are on the order of 1 percent. An alternative approach would have been to use 1 percent for all units. Use of this scaling scheme for estimating fracture porosities is an approximation for determining the spatial variability of porosity among the model layers.

The overall strategy is essentially a combination of the two general approaches available for estimating fracture porosities in the literature. The first approach is based on field tracer transport data. Researchers outside the Yucca Mountain Project have also used similar approaches, which are summarized in *Analysis of Hydrologic Properties Data* (BSC 2003 [DIRS

161773], Section 6.1.3.4). This includes the Apache Leap Research Site (Neuman et al. 2001 [DIRS 160849], p. 320) where an estimated mean fracture porosity of 0.014 was obtained from gas pressure data and fracture porosity estimates of 0.001 to 0.07 from gas tracer tests in the northern Ghost Dance fault in the Yucca Mountain unsaturated zone (LeCain et al. 2000 [DIRS 144612], Table 18).

The second general approach is based on the geometry of a fracture network. This approach considers all the fractures under consideration as connected and requires that fracture apertures can be exactly determined. Although a large degree of uncertainty exists in fracture porosity values estimated from this approach (for several reasons), this approach has often been used when field tracer test data are not available. For example, in their review of numerical approaches for modeling multiphase flow in fractured petroleum reservoirs, Kazemi and Gilman (1993 [DIRS 147209], pp. 270 to 271; pp. 312 to 313) discuss the determination of fracture porosity based on fracture geometry data.

Considering that gas tracer test data are only available for one model layer (tsw34) and a large degree of uncertainty exists when the second approach is used, use of both approaches provides significantly better estimates for fracture porosity in units through the unsaturated zone. A combination of the above two approaches makes the best use of the relevant data.

C.4.2.2.2 Fracture Porosity from Gas Tracer Testing Data

The estimated fracture porosities were developed based on several simplifications (Figure C-7). Flow and transport are two-dimensional; dispersion, gas compressibility, and matrix diffusion are ignored; and the testing medium is homogeneous. The estimations were made using:

$$\phi_f^* = \frac{Qt_{0.5}}{\pi r_L^2 L} \qquad \text{(Eq. C-20)}$$

(BSC 2003 [DIRS 161773], Equation 13) where ϕ_f^* is the estimated fracture porosity, Q is the volumetric withdrawal rate ($Q_{withdrawal}$ in Figure C-9), $t_{0.5}$ is the mean transport time of tracer, r_L is the distance between the tracer injection and withdrawal zones, and L is the length of injection zone. This equation assumes that flow is two-dimensional and confined to a domain of width equal to the length of the injection zone.

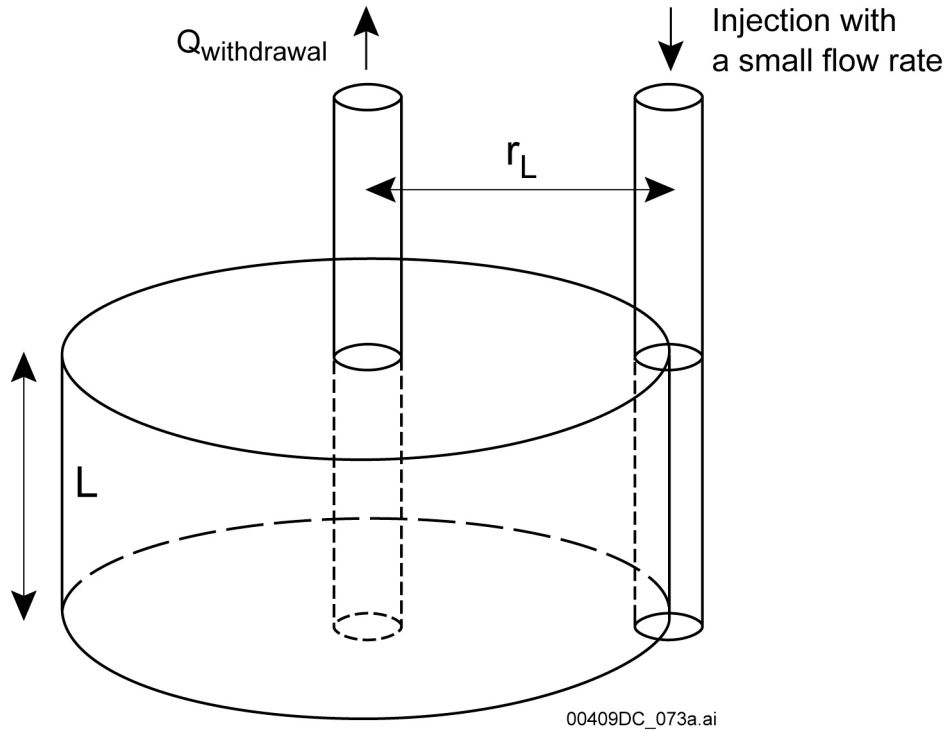

Source: BSC 2003 [DIRS 161773], Figure 3.

Figure C-7. A Conceptual Model for Estimating Fracture Porosity Using Gas Tracer Testing Data

The average fracture porosity, estimated from Equation C-20 using gas tracer data collected from the Drift Scale Test block and Niche 3, is 1.02 _ 10^{-2}.

C.4.2.2.3 Effects of Several Factors on Fracture-Porosity Estimation Based on Gas Tracer Testing Data

The estimation of fracture porosity based on Equation C-20 does not consider the effects of several factors: gas compressibility, heterogeneity, anisotropy, cavities, dispersion, and matrix diffusion. Potential effects of these factors on estimating fracture porosity are in *Analysis of Hydrologic Properties Data* (BSC 2003 [DIRS 161773], Section 6.1.3.3).

The determination of fracture porosity depends on the tracer transport times. Diffusion of trace into the matrix delays the breakthrough and causes overestimation of fracture porosity. Effects of matrix diffusion on the fracture porosity estimation can be quantified by an analytical solution described in *Analysis of Hydrologic Properties Data* (BSC 2003 [DIRS 161773], Section 6.1.3, Equation 23).

$$\frac{\phi_f}{\phi_f^*} = 1 - \frac{t_{0.5}}{\phi_f^*} D_m \left[\frac{A_{fm} \phi_m S_{mg}}{2\beta} \right]^2 V \qquad \text{(Eq. C-21)}$$

where ϕ_f is fracture porosity (considering matrix diffusion), A_{fm} is the fracture–matrix interface area per unit volume of bulk rock, ϕ_m is the matrix porosity, S_{mg} is the gas saturation in the

matrix, and β is a constant (0.48) defined by a *erfc(β)* value of 0.5 and determined from Domenico and Schwartz (1990 [DIRS 100569], p. 637). The ϕ_f and ϕ_f* are identical if matrix diffusion is negligible (using a D_m value of 0), as shown in Equation C-21. This equation can be used to correct the porosity estimates from Equation C-20 to consider the effects of matrix diffusion. Substituting the determined parameter values listed in *Analysis of Hydrologic Properties Data* (BSC 2003 [DIRS 161773], Section 6.1.3.3) into the right hand of Equation C-21 yields (BSC 2003 [DIRS 161773], Equation 26):

$$\frac{\phi_f}{\phi_f *} = 0.83 \qquad \text{(Eq. C-22)}$$

This factor is used to consider the effects of matrix diffusion (on average) by multiplying the porosity estimates by a factor of 0.83. The resultant average fracture porosity for tsw34 is 0.0085, and the corresponding standard deviation is 2.5 _ 10^{-3}. The average porosity and standard deviation were obtained from multiple measurements, described in *Analysis of Hydrologic Properties Data* (BSC 2003 [DIRS 161773], Section 6.1.3.2). This porosity value is used in Equation C-17 for determining fracture porosities in other unsaturated zone model layers. The final fracture-porosity estimates are given in Table C-5.

Fracture-porosity values obtained using different methodologies, based on different types of data and from different sites (described in *Analysis of Hydrologic Properties Data* (BSC 2003 [DIRS 161773], Section 6.1.3.4)), are consistent with the current estimates (given in Table C-5). These estimates are on the order of 1 percent, indicating their reasonableness.

C.4.2.3 Development of Fracture Properties from Field Data

The development of fracture properties from field data is described in *Analysis of Hydrologic Properties Data* (BSC 2003 [DIRS 161773], Section 6.1.2). Fracture frequency and interface area are determined from qualified fracture-property data developed from field data. These include detailed line survey fracture data (collected from the ESF north and south ramps, main drift, and ECRB Cross-Drift, providing spatially varying frequency, length, and fracture dips and strikes) and fracture-frequency data from boreholes.

For calculating fracture frequencies using the detailed line survey in the ESF and ECRB Cross-Drift, the mean fracture frequency is given by the inverse of the mean spacing. The mean spacing is calculated by (BSC 2003 [DIRS 161773], Equation 1):

$$\bar{s} = \frac{1}{nf - 1} \sum_{2}^{nf} \left(D_i - D_{i-1} \right) \qquad \text{(Eq. C-23)}$$

where D_i is the distance or station along the ESF where fracture *i* intersects the detailed line survey and *nf* is the number of fractures. This is the apparent spacing. It is not the normal distance between the center of fractures and is, therefore, a rough estimate of the *true* spacing. These values were not corrected for any possible bias in orientation in the detailed line survey. The mean fracture frequency is given by the inverse of the mean apparent spacing (BSC 2003 [DIRS 161773], Equation 2):

$$\overline{f} = \frac{1}{\overline{s}} \qquad \text{(Eq. C-24)}$$

For calculating fracture frequency from borehole data, the data are processed to normalize for core recovery, corrected for bias in orientation, and scaled to represent larger length fracture. To correct for orientation bias for data from vertical boreholes, dip distributions are used as follows (modified from Lin et al. 1993 [DIRS 116797], p. 24, Equation 3-1) (BSC 2003 [DIRS 161773], Equation 3):

$$f_{cb} = \frac{\sum_i f_{i,0-19° dip}}{\cos(10°)} + \frac{\sum_i f_{i,20-39° dip}}{\cos(30°)} + \frac{\sum_i f_{i,40-59° dip}}{\cos(50°)} + \frac{\sum_i f_{i,60-90° dip}}{\cos(75°)} \qquad \text{(Eq. C-25)}$$

where f_{cb} is the fracture frequency corrected for orientation bias and f_i is the fracture frequency corresponding to the range of dip distribution. Finally, these values are corrected to represent larger length fractures on the scale of those characterized in the ESF. A simple correction ratio is used based on comparisons of ESF data with corresponding vertical boreholes for that model layer (BSC 2003 [DIRS 161773], Equation 4):

$$\overline{f} = f_{corrected} = f_{cb} R$$
$$R = \left(\frac{f_{ESF}}{f_{borehole}} \right)_{average} \qquad \text{(Eq. C-26)}$$

Two correction factors R were calculated, one for welded units using data for the Topopah Spring middle nonlithophysal hydrogeologic unit (tsw34) and one for nonwelded units using data for the Pah Canyon Tuff in the Paintbrush hydrogeologic unit (ptn25). These units were selected because both ESF and borehole data are available; these were considered to be representative of the other units.

The fracture intensity is calculated by dividing the trace length of the fracture by the area surveyed. The area surveyed was 6 m (3 m above and below the traceline) times the length along the tunnel considered for that interval. The average fracture intensity I (m/m^2) is given by (BSC 2003 [DIRS 161773], Equation 5):

$$I = \frac{\sum_{i=1}^{nf} t_i}{\text{area}} = \frac{\sum_{i=1}^{nf} t_i}{(6\text{ m})(\text{interval length in meters})} \qquad \text{(Eq. C-27)}$$

where t_i is trace length in meters for fracture i.

The fracture interface area is calculated by dividing the fracture area by the volume of the interval surveyed. The volume for the interval is estimated by multiplying the interval length surveyed by the square of the geometric mean of surveyed fracture-trace length. The average fracture-interface area per volume A_{fm} (m^2/m^3) is given by (BSC 2003 [DIRS 161773], Equation 6):

$$A_{fm} = \frac{\sum_{i=1}^{nf} \pi r_i^2}{\text{volume}} = \frac{\sum_{i=1}^{nf} \pi r_i^2}{(\text{interval length})(\text{geometric mean of trace lengths})^2} \qquad \text{(Eq. C-28)}$$

where r is the radius of fracture i, or one-half the trace length of fracture i.

Fracture apertures are calculated by the cubic law with the fractures fully connected. The fracture aperture b is then given by Bear et al. (1993 [DIRS 116773], p. 15) (BSC 2003 [DIRS 161773], Equation 7):

$$b = \left(\frac{12k}{\bar{f}} \right)^{1/3} \qquad \text{(Eq. C-29)}$$

where k is the fracture permeability. The fracture aperture determined in this way is an effective hydraulic aperture, not a physical aperture. The k here refers to bulk fracture permeability rather than permeability in a fracture as defined by Bear et al. (1993 [DIRS 116773], p. 15).

The developed fracture properties are given in Table C-5.

C.4.2.4 Fracture–Aperture, Porosity, and Frequency Data in the Abstraction Model

The use of fracture-porosity and spacing data and the estimation of apertures for the abstraction model are described in *Particle Tracking Model and Abstraction of Transport Processes* (BSC 2004 [DIRS 162730], Section 6.5.7). The fracture-porosity and fracture-spacing data are sampled to address the uncertainty of fracture properties on radionuclide transport in TSPA calculations. The data sets list fracture spacing data in terms of fracture frequency, defined as the inverse of fracture spacing. Thus, the fracture frequency is first sampled, and the inverse of the sampled data is taken to derive sampled fracture-spacing data.

Table C-6 lists the uncalibrated fracture-porosity and frequency data based on field information. These are the uncalibrated properties developed in *Calibrated Properties Model* (BSC 2003 [DIRS 160240]). However, fracture-porosity and frequency data are not subject to calibration adjustment in *Calibrated Properties Model* (BSC 2003 [DIRS 160240]); therefore, these properties are carried forward into the calibrated property set without modification.

Table C-6. Fracture-Porosity and Frequency Data

Rock Layer	ϕ_f	Std.	*f* (1/m)	σ_f	Input Description	Type of Uncertainty
tcwf1	2.4×10^{-2}	_	0.92	0.94	ϕ_f is the fracture porosity and *f* is fracture frequency. Data are uncalibrated. However, the fracture-porosity and fracture-frequency data are not subject to adjustment in calibration; therefore, those properties are carried forward into the calibrated property set without modification.	As porosity must fall in the range of 0 and 1, a beta distribution is suitable to describe the uncertainty of the porosity values.
tcwf2	1.7×10^{-2}	_	1.91	2.09		
tcwf3	1.3×10^{-2}	_	2.79	1.43		
ptnf1	9.2×10^{-3}	_	0.67	0.92		
ptnf2	1.0×10^{-2}	_	0.46	_		
ptnf3	2.1×10^{-3}	_	0.57	_		
ptnf4	1.0×10^{-2}	_	0.46	0.45		
ptnf5	5.5×10^{-3}	_	0.52	0.6		
ptnf6	3.1×10^{-3}	_	0.97	0.84		
tswf1	5.0×10^{-3}	_	2.17	2.37		
tswf2	8.3×10^{-3}	_	1.12	1.09		
tswf3	5.8×10^{-3}	_	0.81	1.03		
tswf4	8.5×10^{-3}	2.50×10^{-3}	4.32	3.42		
tswf5	9.6×10^{-3}	_	3.16	_		
tswf6	1.3×10^{-2}	_	4.02	_		
tswf7	1.3×10^{-2}	_	4.02	_		
tswf8/pcf38	1.1×10^{-2}	_	4.36	_		
tswf9/pcf39/tswfz/tswfv	4.3×10^{-3}	_	0.96	_		
ch1fv	6.1×10^{-4}	_	0.10	_		
ch2fv	7.7×10^{-4}	_	0.14	_		
ch3fv	7.7×10^{-4}	_	0.14	_		
ch4fv	7.7×10^{-4}	_	0.14	_		
ch5fv	7.7×10^{-4}	_	0.14	_		
ch6fv	7.7×10^{-4}	_	0.14	_		
ch1fz/pcf1z	1.6×10^{-4}	_	0.04	_		
ch2fz/pcf2z	3.7×10^{-4}	_	0.14	_		
ch3fz	3.7×10^{-4}	_	0.14	_		
ch4fz	3.7×10^{-4}	_	0.14	_		
ch5fz/pcf5z	3.7×10^{-4}	_	0.14	_		
ch6fz/pcf6z	1.6×10^{-4}	_	0.04	_		
pp4f/pcf4p	3.7×10^{-4}	_	0.14	_		
pp3f	9.7×10^{-4}	_	0.20	_		
pp2f	9.7×10^{-4}	_	0.20	_		
pp1f	3.7×10^{-4}	_	0.14	_		
bf3f	9.7×10^{-4}	_	0.20	_		
bf2f	3.7×10^{-4}	_	0.14	_		
tr3f	9.7×10^{-4}	_	0.20	_		
tr2f	3.7×10^{-4}	_	0.14	_		
tcw fault	2.9×10^{-2}	_	1.90	_		
ptn fault	1.1×10^{-2}	_	0.54	_		
tsw fault	2.5×10^{-2}	_	1.70	_		
chn fault	1.0×10^{-3}	_	0.13	_		

Source: BSC 2004 [DIRS 162730], Table 6-11.

Among the listed geologic rock layers, only those below the repository that could affect the transport of radionuclides downward toward the water table are sampled. Rock layers below the repository are grouped together based on similarity in fracture-porosity and frequency characteristics. For groups with multiple units having different parameter values, an arithmetic average value is used for the group. There is only one standard deviation for fracture-porosity, so the other groups are assigned a fracture-porosity standard deviation such that the ratio of the standard deviation to the mean is constant for all the groups. Group 9 (tswf3) has its own standard deviation for fracture frequency, which is used. For the other groups, the standard deviation is set equal to 0.831 times the mean. This is based on the relationship between fracture frequency and the standard deviation of fracture frequency found for model units above the repository (see Figure C-8). In this way, the mean and standard deviation for each parameter in each group was computed.

As porosity must lie within the finite range of 0 to 1, a beta distribution with these bounds is suitable for studying the influence of porosity uncertainty on radionuclide transport Table C-7 lists the distribution data for fracture porosity.

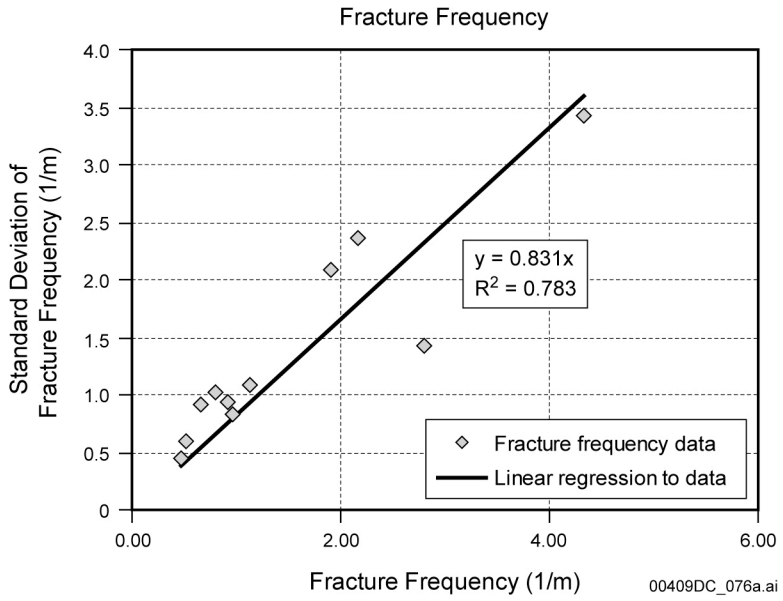

Source: BSC 2004 [DIRS 162730], Figure 6-13.

Figure C-8. Relationship between Fracture Frequency and Standard Deviation

Table C-7. Fracture-Porosity and Frequency Distribution Data

Group	Units	Porosity Beta Distribution min = 0; max = 1		Fracture Frequency (m^{-1})		Fracture Frequency (m^{-1}) Lognormal Distribution		Aperture (m) 2b derived from Eq. C-32: $2b = \frac{\phi_f}{f}$
		Mean	Std	Mean	Std	Mean For ln (f)	Std For ln (f)	
1	chnf	1.0×10^{-3}	3.09×10^{-4}	1.26×10^{-1}	1.05×10^{-1}	_2.42	7.24×10^{-1}	7.94×10^{-3}
2	tswf	2.5×10^{-2}	7.25×10^{-3}	1.75	1.45	2.11×10^{-1}	7.24×10^{-1}	1.43×10^{-2}
3	ch[2,3,4,5]fz	3.7×10^{-4}	1.09×10^{-4}	1.40×10^{-1}	1.16×10^{-1}	_2.31	7.24×10^{-1}	2.64×10^{-3}
	pcf[2,5]z							
	pp4fz							
	pp1fz							
	bf2fz							
	tr2fz							
4	pp3fd	9.7×10^{-4}	2.85×10^{-4}	2.00×10^{-1}	1.66×10^{-1}	_1.96	7.24×10^{-1}	4.85×10^{-3}
	pp2fd							
	bf3fd							
	tr3fd							
5	ch1fz/pcf1z ch6fz/pcf6z	1.6×10^{-4}	4.71×10^{-5}	4.00×10^{-2}	3.32×10^{-2}	_3.57	7.24×10^{-1}	4.00×10^{-3}
6	ch[1,2,3,4,5,6]fv	6.9×10^{-4}	2.03×10^{-4}	1.20×10^{-1}	9.96×10^{-2}	_2.47	7.24×10^{-1}	5.75×10^{-3}
7	tswf9/pcf39 /tswfv/tswfz	4.3×10^{-3}	1.26×10^{-3}	9.60×10^{-1}	7.97×10^{-1}	-3.87×10^{-1}	7.24×10^{-1}	4.48×10^{-3}
8	Tswf[4,5]	1.05×10^{-2}	3.10×10^{-3}	3.97	3.29	1.03	7.24×10^{-1}	2.64×10^{-3}
	tswf[6,7]							
	tswf8/pcf38							
9	tswf3	5.8×10^{-3}	1.71×10^{-3}	8.10×10^{-1}	1.03	-6.92×10^{-1}	9.81×10^{-1}	7.16×10^{-3}

Source: BSC 2004 [DIRS 162730], Table 6-13.

Given that fracture frequency can theoretically span values from zero to infinity, the lognormal distribution is suitable. The mean and standard deviation for $\ln(f)$ are given in terms of the mean and standard deviation for f by the following relationships from Hogg and Craig (1978 [DIRS 163236], pp. 180 and 432) (BSC 2004 [DIRS 162730], Equations 6-24 and 6-25):

$$\mu_{\ln(f)} = \ln(\mu_f) - \frac{1}{2}\ln\left(1 + \frac{\sigma_f^2}{\mu_f^2}\right) \quad \text{(Eq. C-30)}$$

$$\sigma_{\ln(f)} = \sqrt{\ln\left(1 + \frac{\sigma_f^2}{\mu_f^2}\right)} \quad \text{(Eq. C-31)}$$

For further information on this derivation, see *Drift-Scale Radionuclide Transport* (BSC 2003 [DIRS 164889], Attachments I and XI, equations I-1, I-2, and XI-4 through XI-7.) Values for $\mu_{\ln(f)}$ and $\sigma_{\ln(f)}$ are given in Table C-7.

In TSPA-LA calculations, fracture porosity and fracture frequency are sampled independently. The basis for this approximation is that there is only a very weak correlation between fracture porosity and frequency (BSC 2004 [DIRS 162730], Figure 6-14). Therefore, correlating these two parameters is not warranted.

The sampled fracture-porosity and frequency data are used in deriving the fracture spacing and aperture based on the following relationship (BSC 2004 [DIRS 162730], Equation 6-26):

$$\phi_f = (2b)f \qquad \text{(Eq. C-32)}$$

where $2b$ is the fracture aperture (m), f is the fracture frequency (m^{-1}), and ϕ_f is the fracture porosity. Fracture frequency is the inverse of the fracture spacing.

C.4.2.5 Residual Saturation and the Active-Fracture Model _ Parameter Values for the Abstraction Model

Fracture residual saturation and fracture _ parameter values are used by FEHM to calculate the fracture spacing based on the active-fracture model (Liu et al. 1998 [DIRS 105729]). In TSPA-LA, a constant fracture residual saturation of 0.01 is used for all layers (BSC 2004 [DIRS 162730], Section 6.5.6). Values for fracture parameter _ and their sources are tabulated for the lower-bound, mean, and upper-bound infiltration scenarios for the model layers in Tables C-2 to C-4 (BSC 2004 [DIRS 162730], Tables 6-8 to 6-10).

C.4.3 Adaptation of the Active-Fracture Model for Abstraction Transport Model Calculations

The fracture_matrix interaction submodel of the transport model is described in *Particle Tracking Model and Abstraction of Transport Processes* (BSC 2004 [DIRS 162730], Section 6.4.3) and derived in *Particle Tracking Model and Abstraction of Transport Processes* (BSC 2004 [DIRS 162730], Section III-1). The governing equations required for the fracture–matrix interaction submodel is a solute transport system in a domain consisting of parallel flow in a fracture and adjacent matrix, with fracture–matrix solute interaction via molecular diffusion in the rock matrix. For simplicity, longitudinal dispersion is not considered in either medium, advection is considered only in the z direction, and diffusion is considered only normal to the flow direction. The rationales for these simplifications are as follows. With regard to longitudinal dispersion, this submodel is intended only to capture the impact of diffusion because dispersion is captured separately in the particle tracking algorithm. Likewise, the advection from fracture to matrix (or the reverse) is separately implemented in the particle tracking algorithm. Therefore, the remaining processes to be included as part of the transfer functions are advection and diffusion in the z-direction only.

The transport equation for the fracture is derived from first principles to demonstrate the means by which terms in the dimensionless groups must be altered to include the effects of the active-fracture model. Taking a control volume in the fracture of width b (half of the full aperture), depth d, and length Δz, the following terms of the transient solute mass balance (units of each of these terms are solute mass per time) are (BSC 2004 [DIRS 162730], Equation III-1):

$$bd\Delta z\theta_f R_f \frac{(C - C_{prev})}{\Delta t} \qquad \text{(Eq. C-33)}$$

where C_{prev} represents the concentration at the previous time step, θ_f is the volumetric water content in the fracture, and R_f is the fracture retardation factor. For advection (BSC 2004 [DIRS 162730], Equation III-2):

$$bd\overline{V}_z(C_{z+\Delta z} - C_z) \qquad \text{(Eq. C-34)}$$

where $\overline{V}_z$ is the Darcy velocity in the fracture, equal to volumetric flow rate divided by the total cross-sectional area in the fracture. For diffusion into matrix (BSC 2004 [DIRS 162730], Equation III-3):

$$d\Delta z\theta_m D_m \left.\frac{\partial C_m}{\partial x}\right|_{x=b} \qquad \text{(Eq. C-35)}$$

where D_m is the effective diffusion coefficient in the matrix and θ_m is the matrix volumetric water content. These terms form the overall solute mass balance equation (BSC 2004 [DIRS 162730], Equation III-4):

$$bd\Delta z\theta_f R_f \frac{(C - C_{prev})}{\Delta t} = -bd\overline{V}_z(C_{z+\Delta z} - C_z) + d\Delta z\theta_m D_m \left.\frac{\partial C_m}{\partial x}\right|_{x=b} \qquad \text{(Eq. C-36)}$$

Dividing by $bd\Delta z\theta_f$, making use of the relation for the fracture-interstitial pore-water velocity $V_f = \overline{V}_z / \theta_f$, and taking the limit as Δz and Δt go to 0, yields (BSC 2004 [DIRS 162730], Equation III-7):

$$R_f \frac{\partial C_f}{\partial t} = -V_f \frac{\partial C_f}{\partial z} + \left.\frac{\theta_m D_m}{\theta_f b}\frac{\partial C_m}{\partial x}\right|_{x=b} \qquad \text{(Eq. C-37)}$$

The subscript *f* on the concentration denotes the fracture.

Given the assumptions listed at the beginning of this derivation, the differential equation governing transport in the matrix is (BSC 2004 [DIRS 162730], Equation III-8):

$$R_m \frac{\partial C_m}{\partial t} = D_m \frac{\partial^2 C_m}{\partial x^2} - V_m \frac{\partial C_m}{\partial z} \quad \text{(Eq. C-38)}$$

where V_m is the interstitial pore-water velocity in the matrix, and D_m is the matrix retardation factor.

In the active-fracture model of Liu et al. (1998 [DIRS 105729]), the fraction of the connected fractures in a network that flow, f_a, is expressed as (BSC 2003 [DIRS 161773], Equation 52):

$$f_a = S_e^{\gamma} \quad \text{(Eq. C-39)}$$

where _ is a positive constant depending on properties of the corresponding fracture network, and the effective water saturation in connected fractures is given by (BSC 2003 [DIRS 161773], Equation 53)

$$S_e = \frac{S_f - S_r}{1 - S_r} \quad \text{(Eq. C-40)}$$

where S_f is the water saturation of all connected fractures and S_r is the residual fracture saturation.

The active-fracture model requires that adjustments be applied to the interface area and the mean spacing between flowing fractures. These adjusted parameters can then be used in the transport model calculations. Examining the individual terms of the mass balance for the fracture, the accumulation term (Equation C-33) is unchanged by the active-fracture model, because it is based on the storage volume in the fracture, as well as sorption parameters. Storage volumes in the dual-k flow fields are fully defined by the fracture volume fractions and the fluid saturations in the fracture continuum. Fluid saturations are model output from the flow simulations, and no further correction for transport is required for the accumulation term. Likewise, the Darcy velocity in the advection term (Equation C-34) is fully defined by the flux through the fracture continuum, so no active-fracture model corrections are required for advection either.

The diffusion term (Equation C-35) consists of a flux $\theta_m D_m \left.\frac{\partial C_m}{\partial x}\right|_{x=b}$ times an interfacial area. This interfacial area term, according to the active fracture model, should be reduced to account for the fact that not all fractures are flowing. Liu et al. (1998 [DIRS 105729], Equation 12) give the following reduction factor for correcting the advective flux term (nomenclature from Liu et al. 1998 [DIRS 105729] is used in this equation) (BSC 2004 [DIRS 162730], Equation III-34):

$$R = \left(\frac{A_{fm,a}}{A_{fm}}\right)\left(\frac{n_{f,a}}{n_f}\right)\left(\frac{d}{d_a}\right) \quad \text{(Eq. C-41)}$$

Although Liu et al. (1998 [DIRS 105729]) refer to R as the fracture–matrix interface area reduction factor, it is clear from their derivation that the term represents the ratio of the fluxes for the uncorrected and corrected cases, correcting for both the interface area and the transport length scale associated with the distance between the flowing fractures (the third term on the right-hand side of this equation). Therefore, in the FEHM simulations, active-fracture model-based adjustments should be applied to both the interface area and the spacing B. The term d/d_a is the adjustment to the fracture spacing, where d is the fracture spacing, and d_a is the fracture spacing in the active-fracture continuum, and is described by the following relation (Liu et al. 1998 [DIRS 105729], Equation 17) (BSC 2004 [DIRS 162730], Equation III-35):

$$\frac{d}{d_a} = S_e^{\gamma} \qquad \text{(Eq. C-42)}$$

Thus, the geometric spacing B in the FEHM transport simulations is multiplied by S_e^{γ} to obtain the spacing between flowing fractures.

The interface-area portion of the adjustment consists of the first two terms on the right hand side of Equation C-41, the first to account for the reduction in wetted area within an individual fracture, and the second to account for the reduction in area associated with a smaller number of wetted fractures. This term can be related to the active-fracture model parameters using Equations 13 and 14 of Liu et al. (1998 [DIRS 105729]) (BSC 2004 [DIRS 162730], Equation III-36):

$$\left(\frac{A_{fm,a}}{A_{fm}}\right)\left(\frac{n_{f,a}}{n_f}\right) = S_e^{1-\gamma} S_e^{\gamma} = S_e \qquad \text{(Eq. C-43)}$$

To implement this area reduction term in FEHM, the geometrically defined aperture b is divided by S_e. The adjustment to b is for convenience and actually arises from the need to adjust the interface area in the fracture-transport equation.

Fracture-hydraulic properties in the process model and the constitutive relationships are defined for active fractures as a function of the effective water saturation of active fractures. This is related to the effective water saturation in connected fractures, S_e, by (BSC 2003 [DIRS 161773], Equation 54):

$$S_{ae} = \frac{S_e}{f_a} = S_e^{1-\gamma} \qquad \text{(Eq. C-44)}$$

Because $S_{ae} \leq 1$, _ should be in a range between 0 and 1. The effective water saturation of active fractures is related to the actual water saturation in active fractures, S_a, by (BSC 2003 [DIRS 161773], Equation 55):

$$S_{ae} = \frac{S_a - S_r}{1 - S_r} \qquad \text{(Eq. C-45)}$$

However, the volumetric water content used in Equations C-35 through C-37 is not modified for the active-fracture model formulation because it is equal to the product of S_e (for all the connected fractures) and fracture porosity.

C.4.4 Verification of the Active-Fracture Model with Matrix Diffusion in the Abstraction Model

Particle Tracking Model and Abstraction of Transport Processes (BSC 2004 [DIRS 162730], Section 6.4.3) describes the fracture–matrix interaction submodel. For transport in a dual-permeability system at the field scale, the flow model consists of one matrix grid cell for each fracture cell. However, important processes associated with flow and transport occur at scales smaller than those considered in the mountain-scale unsaturated zone model, particularly in the immediate region of the matrix adjacent to each flowing fracture. Therefore, the incorporation of fracture–matrix interactions into the model is, in essence, an upscaling problem. The goal of this development is to utilize a suitable idealized system that captures, at the small scale, important transport processes and allows this small-scale behavior to be simply upscaled for inclusion in the large-scale model. As demonstrated below (taken from *Particle Tracking Model and Abstraction of Transport Processes* (BSC 2004 [DIRS 162730], Section 6.4.3)), this upscaling method will allow testing of alternate conceptual models for the fracture–matrix interaction model for transport.

To accomplish the upscaling within the particle tracking transport model, the transfer function approach is used, constructing an idealized transport model at the small scale that allows the transfer functions to be tabulated. In a dual-permeability system, transport behavior is vastly different depending on whether solute starts in the fracture or in the matrix. Therefore, the transfer function method is adapted in the unsaturated zone transport model to accommodate dual-permeability behavior.

The approach consists of using transfer functions to determine both the residence time in a cell and whether the particle enters the next cell in the fractures or the matrix. In this way, the combined fracture and matrix system will be treated as a unified medium in which there is a distribution of transport times depending on whether the particle enters the cells in the fracture versus the matrix. The transfer functions themselves (described below and in Attachment III of *Particle Tracking Model and Abstraction of Transport Processes* (BSC 2004 [DIRS 162730]) are computed based on an idealized fracture–matrix transport model with parallel flow in the fractures and matrix. The steps of the algorithm are as follows (the algorithm starts with a known particle location, either in the fracture or matrix continuum):

1. Determine probabilistically whether the particle should move to the other medium due to advective flux to that medium.

2. Determine probabilistically whether the particle will leave this cell via the current medium or the other medium.

3. Use the conditional transfer function to determine probabilistically the residence time of the particle.

4. Determine probabilistically which cell the particle moves to next (whether it starts in the fracture or matrix continuum in the next cell has been determined previously in step 2) using the relative total flux to adjacent nodes.

This approach handles the combined fracture and matrix continua as a single porous medium through which mass travels and apportions the particles to each continuum according to the diffusive and advective fluxes defined by the flow field and the transport parameters. In the most general case, the dual-permeability flow model at the mountain scale prescribes a net flow through the fracture continuum, a net flow through the matrix continuum, and a fracture-to-matrix (or matrix-to-fracture) fluid flux. To implement this algorithm and allow the transfer function to be computed readily, step 1 takes the fracture–matrix advective flux term and applies it immediately when the particle enters the cell. Then, after potentially shifting the particle from one medium to the other via advection (with no increase to the transport time) the subsequent transfer functions are based on parallel flow in the two continua with no flux between the continua.

This approach, which amounts to a form of upwinding of the fracture–matrix fluid flux term, simplifies the transfer function process by eliminating the need for an additional variable, the fracture–matrix advective flux, in the construction of the transfer function curves. Instead, a probability p_{fm} of the particle transferring to the other medium (step 1) is assigned as

- $p_{fm} = 0$ if the fracture–matrix flux term f_{fm} is into the medium in which the particle already resides,
- $p_{fm} = f_{fm}/(f_{fm} + f_{in})$, where f_{in} is the total flux into the continuum in which the particle currently resides.

Step 2 accounts for the fact that there is a finite probability that, due to matrix diffusion, the particle will leave the cell through the other medium regardless of where it originates. In the transfer function approach, solute mass is introduced in the model system (the two-dimensional discrete fracture model) in either the fracture fluid or the matrix fluid. For the general case of water flow through both the fracture and matrix, mass leaves the discrete fracture model via either medium. Therefore, conditional transfer functions must be generated to obtain the probabilities in step 2. That is, for mass injected with the fracture fluid entering the discrete fracture submodel, there is a breakthrough curve for mass leaving the model via the fracture fluid, and a similar breakthrough curve for mass leaving via the matrix fluid.

Similarly, there are two breakthrough curves for mass injected with the matrix fluid. The plateau values attained for a given transfer function curve represents the probability of leaving via a particular medium in step 2. In other words, the probability of a particle leaving via a given continuum equals the steady-state solute mass flux (the plateau of the transfer function curve) divided by the total mass flux through the discrete fracture model. This step provides a way to assign probabilities for moving particles between the media via diffusion in a system in which water flows through both continua.

Once step 2 is completed using the steady-state solute mass flux derived from the conditional transfer functions, the transfer function to apply to obtain the residence time for step 3 becomes

known. This part of the method is identical to that described previously, which involves generating a random number between 0 and 1 and determining the particle residence time from the transfer function.

Finally, step 4 routes the particle to the appropriate connecting cell in the finite volume domain, as described earlier. If the particle is determined to enter an adjoining cell via the fracture continuum, then the internodal fluxes associated with the fractures are used to define the probabilities of traveling to each connected fracture cell. Similarly, for transport to an adjoining matrix cell, matrix fluxes are used.

The process employed in this model to obtain the transfer functions for the dual permeability transport submodel consists of a series of numerical simulations on the idealized model system shown in Figure C-9. Because each gridblock in the mountain-scale model possesses different hydrologic and transport parameters, a procedure for deriving a nondimensional form of the submodel is required to make the method practical. *Particle Tracking Model and Abstraction of Transport Processes* (BSC 2004 [DIRS 162730], Attachment III) presents the derivation of the nondimensional model and presents the method for generating the transfer function curves. In summary, there are three nondimensional groups that, if specified, fully capture the range of behavior of the submodel (BSC 2004 [DIRS 162730], Equations 6-9 to 6-11):

$$p_1 = \frac{D_m \tau_f R_f}{B^2 R_m} \quad \text{(Eq. C-46)}$$

$$p_2 = \frac{D_m \tau_f \theta_m}{bB\theta_f} \quad \text{(Eq. C-47)}$$

$$p_3 = \frac{\tau_f R_f}{\tau_m R_m} \quad \text{(Eq. C-48)}$$

In these equations, D_m is the effective diffusion coefficient; τ_f and τ_m are the fluid transport times in the fracture and matrix, respectively; R_f and R_m are the retardation factors in the fracture and matrix, respectively; B is the half-spacing between flowing fractures; b is the fracture half-aperture; and θ_f and θ_m are the volumetric water contents of the fracture and matrix, respectively. For a given parameter vector (p_1, p_2, p_3), there is a unique set of conditional transfer function curves of the form $\hat{C}$ versus $\hat{t}$, where $\hat{C}$ is the normalized breakthrough curve for the nondimensional time $\hat{t}$ given by (BSC 2004 [DIRS 162730], Equation 6-12):

$$\hat{t} = \frac{t}{R_f \tau_f} \quad \text{(Eq. C-49)}$$

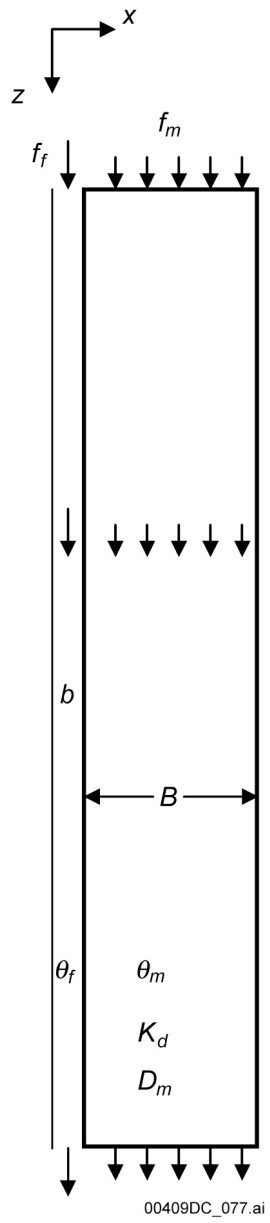

Source: BSC 2004 [DIRS 162730], Figure 6-5.

Figure C-9. Schematic of the Fracture-Transport Submodel

The set of conditional transfer function curves consists of a total of four normalized curves for each (p_1, p_2, p_3): mass input in fracture, output in fracture; mass input in fracture, output in matrix; mass input in matrix, output in fracture; and mass input in matrix, output in matrix. This capability for sampling conditional transfer functions associated with the fracture–matrix interaction dual permeability submodel of the unsaturated zone transport abstraction model has been implemented and documented in FEHM V2.21 (LANL 2003 [DIRS 165741]).

The final issue associated with implementing the transfer function approach is the means by which the idealized model of Figure C-9 is simulated. Two alternative conceptual models are

implemented in this abstraction model to simulate different types of fracture–matrix interaction conceptualizations. In the first alternative conceptual model, called the discrete fracture model formulation, a two-dimensional numerical grid is used with fine discretization in the matrix close to the fracture. This allows sharp gradients in concentration close to the fracture to be captured. The second alternative conceptual model, called the dual-k formulation, uses a numerical grid with one finite volume cell that is paired with each fracture grid cell. This type of discretization is identical to that used in the dual-k transport formulation of the T2R3D process model.

It could be argued that the discrete fracture model formulation more accurately captures the small-scale transport processes. However, the dual-k formulation has the advantage of consistency with the model formulation on which the flow simulations are based. Furthermore, as a practical matter, the three-dimensional process model uses a dual-k formulation for transport, so, for benchmarking purposes, the dual-k approach is more likely to yield comparable results.

In *Particle Tracking Model and Abstraction of Transport Processes* (BSC 2004 [DIRS 162730], Section 7), the implementation of the active-fracture model in the abstraction model was shown to reproduce the qualitative features of the breakthrough curves documented in the reports on which this abstraction is based. Thus, the abstraction model has been compared in the full complexity of the unsaturated zone model and found to be able to represent the system robustly and efficiently for the entire range of parameters and conceptual models required. The following tests were documented in *Particle Tracking Model and Abstraction of Transport Processes* (BSC 2004 [DIRS 162730], Section 7).

C.4.4.1 Comparison of the Particle Tracking Model with Simulations in a Two-Dimensional Cross-Sectional Model

Particle Tracking Model and Abstraction of Transport Processes (BSC 2004 [DIRS 162730], Section 7.2) describes the comparison of the particle tracking model for abstraction with simulations from *Radionuclide Transport Models Under Ambient Conditions* (BSC 2003 [DIRS 163228]) using T2R3D in a two-dimensional cross-sectional model. The particle tracking model tests two alternative conceptual models to describe fracture–matrix interactions: the discrete fracture model and the dual-k formulation. The T2R3D process model uses both the dual-k and MINC formulations. *Radionuclide Transport Models Under Ambient Conditions* (BSC 2003 [DIRS 163228]) showed that these formulations, which constitute alternative conceptual models for transport, can produce significantly different results.

Two alternative conceptual models have been developed on the two-dimensional cross-sectional model using T2R3D. The simulations called dual-k use a finite-volume dual-permeability model formulation in which the fracture–matrix diffusion term is governed by a simple gradient calculated as the difference in concentration between the media divided by a characteristic distance, on the order of the flowing fracture spacing. In addition, in *Radionuclide Transport Models Under Ambient Conditions* (BSC 2003 [DIRS 163228]), the MINC conceptual model employs a series of gridblocks in the matrix.

The unsaturated zone abstraction model implemented in FEHM is capable of simulating either situation. In the conceptualization termed the discrete fracture model fracture–matrix interaction

model, sharp concentration gradients are captured through use of a transfer function obtained using a discrete fracture model with fine discretization in the matrix, analogous to a MINC formulation. By contrast, a dual-k model can be used to generate transfer functions, and those results might be expected to resemble those of T2R3D when an analogous dual-k formulation is used.

In all abstraction model cases, the flow field on which the transport model is run is a dual-k flow field because the particle tracking abstraction model was formulated with the dual-k flow assumption. Therefore, the transport runs with the discrete fracture model formulation for the fracture–matrix interaction submodel employ a finely discretized matrix block for transport but a single matrix block for the flow field. This approach should enable sharp gradients likely to be present for solute transport to be captured in the model.

Figure C-10 plots the comparison results of the particle tracking model and the two alternative conceptual models simulated with T2R3D. For the case of no diffusion, there is excellent agreement between the particle tracking model and the dual-k, no-diffusion model using T2R3D. Slight differences may be attributable to subtle differences in model formulation, numerical errors for one or the other model, or the fact that 1 of the 11 nodes designated as a repository node in the T2R3D runs was omitted from the particle tracking runs because it was found to be located in the PTn. Even with these possible sources for the difference, the agreement provides confidence that particle routing and transit times are properly implemented.

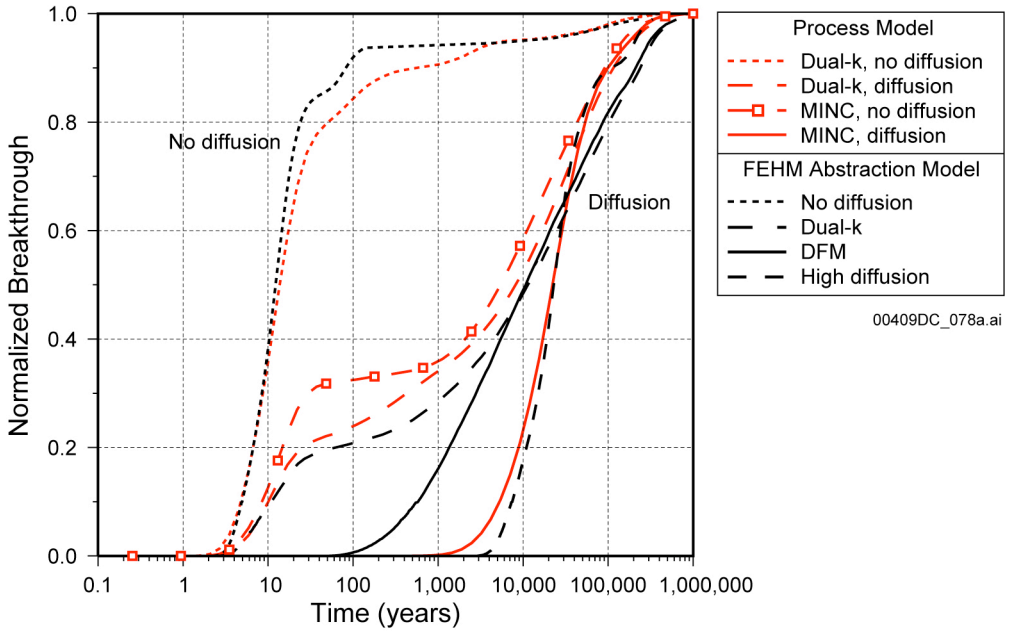

Source: BSC 2004 [DIRS 162730], Figure 7-9.

Figure C-10. Comparison of the Particle Tracking Model with Process Models for a Two-Dimensional, Mountain Scale Model, with and without Diffusion, for Dual-k and Discrete Fracture Model Formulations for the Fracture–Matrix Interaction Model

The mismatch between the MINC, no diffusion and the dual-k simulations (both T2R3D and particle tracking) indicates that there are differences in the flow regime for the MINC model.

The reasons for this difference stem from the fact that the numerical discretization of this model is different than that of the dual-k model. Because of differences in the flow regimes of the MINC and dual-k flow models, the particle tracking runs, which input the dual-k flow field rather than the MINC flow field, are not expected to match the MINC results precisely. Nevertheless, the particle tracking and MINC models are expected to predict similar breakthrough curve features when the former are computed with the discrete fracture model conceptual model transfer function curves. By contrast, diffusion in the dual-k transport model is expected to predict much earlier breakthrough of a portion of the solute mass.

The simulations with diffusion in Figure C-10 confirm this result. In this figure, various FEHM particle tracking simulations are benchmarked against simulations using a dual-k or MINC formulation for the two-dimensional cross section. The difference in predicted behavior between the two conceptual models is reflected in the FEHM simulations in a manner similar to that of the process models. Comparing the MINC and FEHM discrete fracture models, first arrivals in both cases occur much later in time than for the dual-k models.

For comparison, a high-diffusion case is also presented to illustrate the upper limit of breakthrough times for this flow field. Regarding the dual-k models, the characteristic feature of early arrival of a significant portion of the mass at times similar to that of pure fracture transport is produced in both the process and abstraction models. The fraction of the mass arriving early is somewhat lower in the FEHM model than in the T2R3D model, but qualitatively, the dual-k transfer function curves yield behavior quite similar to the process model result using T2R3D. Also, both the process model and abstraction model results converge at longer transport times, regardless of the formulation of the fracture–matrix interaction model or the value of diffusion coefficient used. Finally, the high-diffusion FEHM simulation is shown to bracket the behavior of the breakthrough curves in the figure, with results that are very close to that of the MINC model.

All of these indicators show that the abstraction model compares adequately with the process models and properly accounts for the role of conceptual model uncertainty in the fracture–matrix interaction model. The relatively minor differences of the models employing the dual-k fracture–matrix conceptual model are probably attributable to subtle differences in model formulation and mathematical techniques for solving the transport problem.

C.4.4.2 Comparisons with the Full Three-Dimensional Transport Model Being Used in Total System Performance Assessment for License Application

In *Particle Tracking Model and Abstraction of Transport Processes* (BSC 2004 [DIRS 162730], Section 7.3), the full complexity of the unsaturated zone in terms of heterogeneities in fluid flow conditions and properties is considered using comparisons with the full three-dimensional transport model used in TSPA-LA. The radionuclide ^{99}Tc is released at the repository horizon, and the breakthrough at the water table is recorded and compared to results from T2R3D, documented in *Radionuclide Transport Models Under Ambient Conditions* (BSC 2003 [DIRS 163228]).

C.4.4.2.1 Comparisons of FEHM and T2R3D for the Dual-k Conceptual Model

The comparison of FEHM and T2R3D for the dual-k conceptual model is discussed in Section 7.4 and shown in Figure 7-2. The cumulative transport time distributions through the unsaturated zone for ^{99}Tc for the two models' three flow fields (lower, mean, and upper) show excellent agreement, considering the vast range of infiltration conditions covered in these comparisons. This agreement demonstrates that all significant features of the unsaturated zone transport system are captured with the abstraction model.

C.4.4.2.2 Influence of Diffusion Coefficient and Fracture–Matrix Interaction Alternate Conceptual Model

Figure C-11 shows the behavior of the FEHM model over the complete range of diffusion coefficients, from no diffusion to a case in which diffusion is set so high that it effectively yields a composite medium behavior. The envelope of behavior as a function of diffusion is quite large, whereas the behavior of T2R3D is reproduced when the same parameters and conceptual model for fracture–matrix interactions is selected. This result illustrates that the abstraction model yields reasonable results over a wide range of diffusion coefficients, one of the key parameter uncertainties in the TSPA model.

Also shown in Figure C-11 is the predicted behavior using the discrete fracture model formulation for the fracture–matrix interaction model. No process model results are available for comparison due to the computational limitations of simulating the full three-dimensional model using a MINC formulation. The results are reasonable, given the model behavior shown in Figure C-10 for the smaller two-dimensional cross-sectional model. The main differences for these alternative conceptual models are at the earliest arrival times, where the dual-k model predicts much faster arrivals at the water table. For later transport times the two curves track each other closely, showing that the results are insensitive to the conceptual model. Finally, all breakthrough curves with diffusion, including the high-diffusion case, converge at large transport times. This result is also reasonable, providing additional evidence for the correct functioning of the fracture–matrix interaction model.

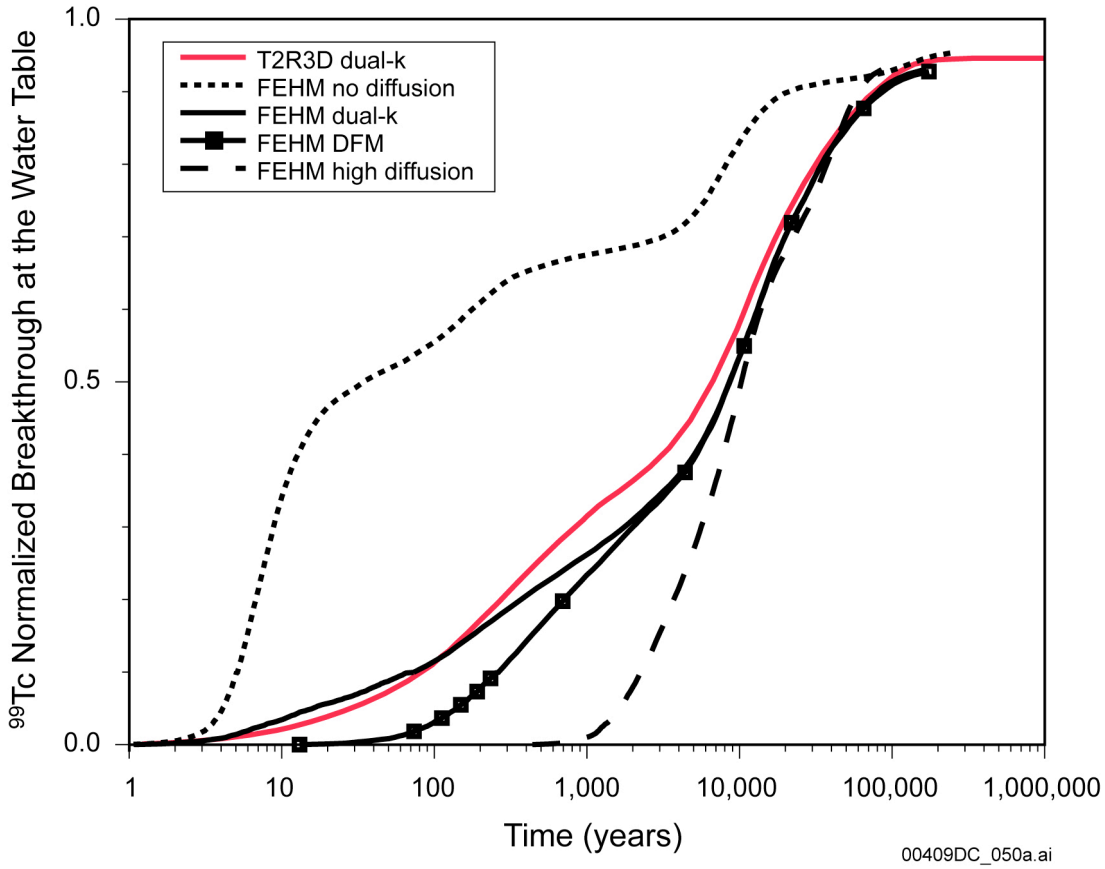

Source: BSC 2004 [DIRS 162730], Figure 7-11.

Figure C-11. Comparison of Breakthrough Curves for ^{99}Tc for T2R3D and the Unsaturated Zone Transport Abstraction Model: Mean Infiltration Scenario, Diffusion in FEHM Ranging from No Diffusion to High Values

C.4.4.2.3 Tests of the Active-Fracture Model Implementation

Simulations for a range of active-fracture model _ parameters show that the active-fracture model formulation in FEHM yields results similar to that of the process model. Process flow model results (BSC 2003 [DIRS 163045], Section 6.8.1) have demonstrated that the active-fracture model parameters have very little influence on the flow field. Therefore, active-fracture model parameter changes to the transport model can be applied using flow model results obtained from the base-case flow simulation.

Figure C-12 illustrates the impact of lowering the _ parameter in the same fashion as was done in *UZ Flow Models and Submodels* (BSC 2003 [DIRS 163045], Section 6.8.2, Figure 6.8-3) and in Figure C-13. Lowering the _ parameter in the TSw in the same manner as in *UZ Flow Models and Submodels* (BSC 2003 [DIRS 163045]) yields a trend toward longer arrival times for the earliest arriving solute for both models. The curves converge at longer transport times. The fact that the lowering of _ in additional units below the repository has no further effect indicates that the principal sensitivity is for the alternate fracture model parameters in the TSw. For the purposes of the abstraction model validation, this qualitative comparison to the results of in

Figure C-13 provides strong evidence that the implementation in FEHM with respect to the alternate fracture model replicates the behavior of the process model.

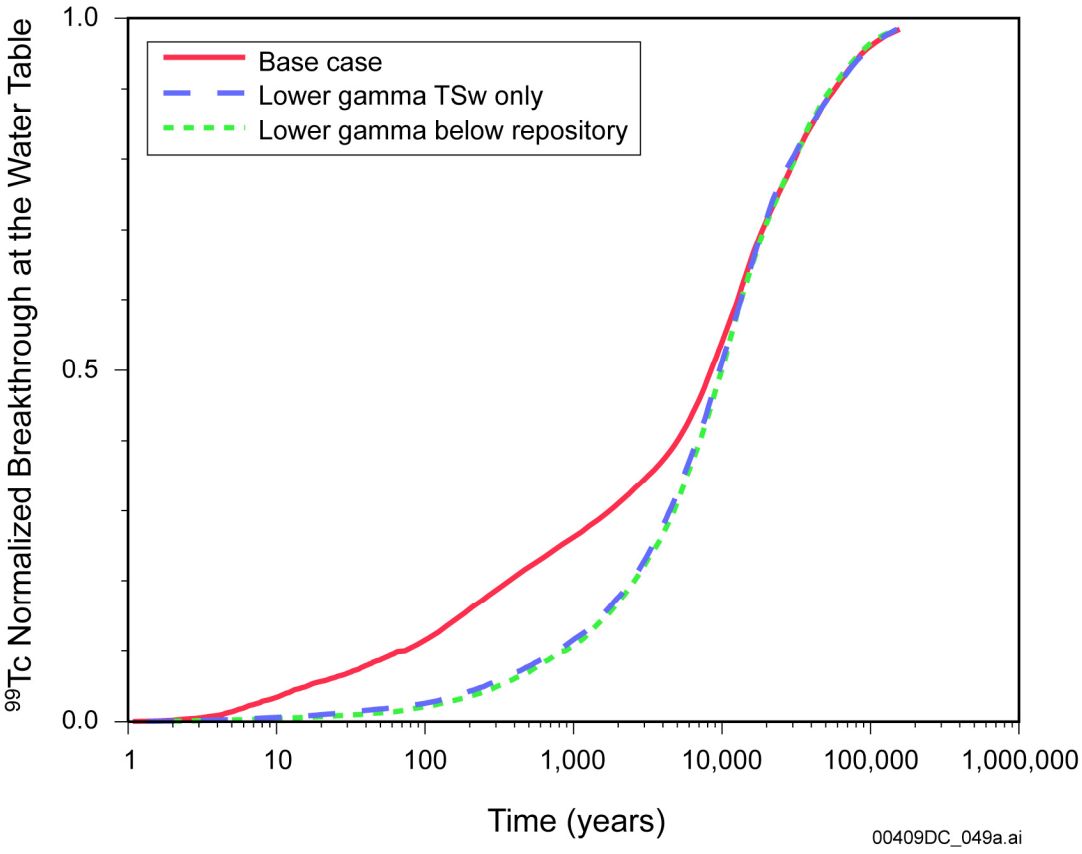

Source: BSC 2004 [DIRS 162730], Figure 7-13.

NOTE: The colors, line types, and legend descriptors were chosen to facilitate a direct visual comparison to the simulation results presented in *UZ Flow Models and Submodels* (BSC 2003 [DIRS 163045], Figure 6.8-3), (see Figure C-13).

Figure C-12. Breakthrough Curves for Conservative Solute Using the Unsaturated Zone Transport Abstraction Model to Investigate the Role of Alternate Fracture Model Parameter _: Dual-k Alternate Conceptual Model, Simulation for Different Values of _ in Rock Units beneath the Repository

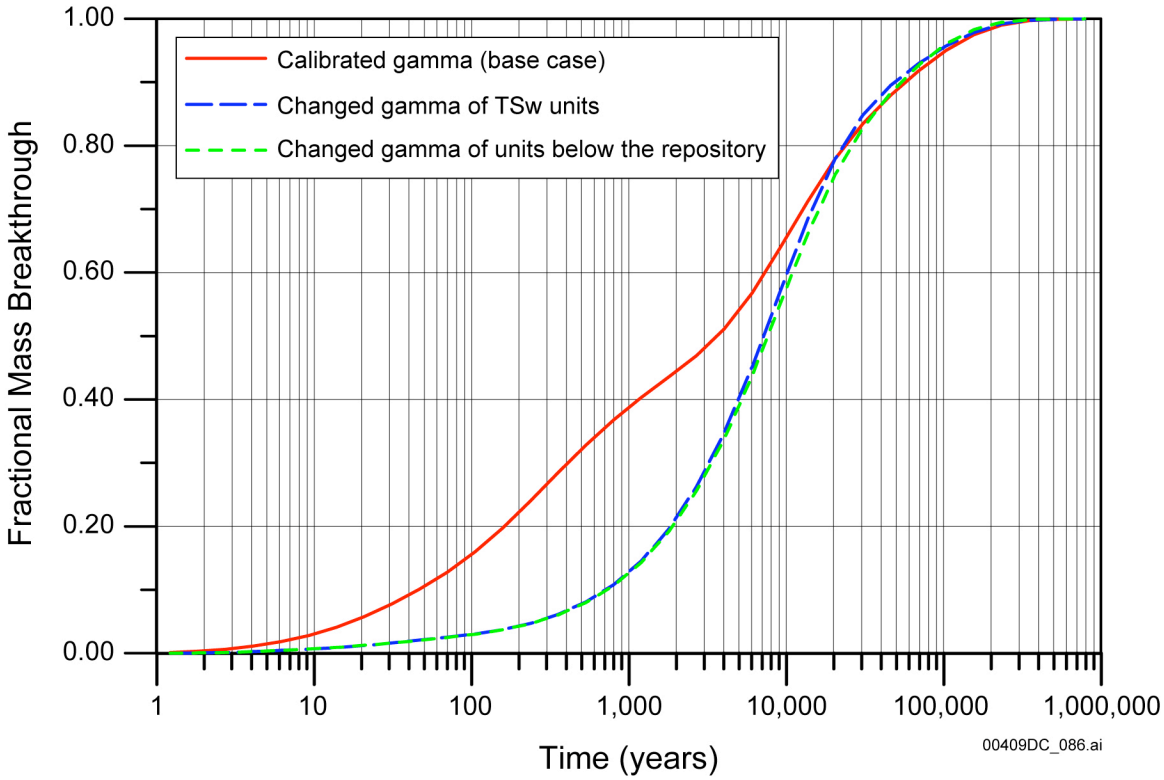

Source: BSC 2003 [DIRS 163045], Section 6.8, Figure 6.8-3.

NOTE: Red solid line = calibrated rock hydraulic properties; blue dashed line = smaller _ of TSw units; green solid line = smaller _ of all units below the repository.

Figure C-13. Comparison of a Simulated Breakthrough Curve of Relative Radionuclide Mass at the Groundwater Table Obtained for the Base Case (using Calibrated Rock Hydraulic Properties), a Case Using a Smaller (Half) _ of the TSw units, and Another Case Using a Smaller (Half) Value of _ of All Units below the Repository

C.5 REFERENCES

C.5.1 Documents Cited

116773 Bear, J.; Tsang, C.F.; and de Marsily, G., eds. 1993. *Flow and Contaminant Transport in Fractured Rock.* San Diego, California: Academic Press. TIC: 235461.

156915 Brooks, R.H. and Corey, A.T. 1964. *Hydraulic Properties of Porous Media.* Hydrology Paper No. 3. Fort Collins, Colorado: Colorado State University. TIC: 217453.

159725 BSC (Bechtel SAIC Company) 2001. *Analysis of Hydrologic Properties Data.* ANL-NBS-HS-000002 REV 00 ICN 01. Las Vegas, Nevada: Bechtel SAIC Company. ACC: MOL.20020429.0296.

160247 BSC 2002. *Analysis of Geochemical Data for the Unsaturated Zone*. ANL-NBS-HS-000017 REV 00 ICN 02. Las Vegas, Nevada: Bechtel SAIC Company. ACC: MOL.20020314.0051.

160240 BSC 2003. *Calibrated Properties Model*. MDL-NBS-HS-000003 REV 01. Las Vegas, Nevada: Bechtel SAIC Company. ACC: DOC.20030219.0001.

161773 BSC 2003. *Analysis of Hydrologic Properties Data*. MDL-NBS-HS-000014 REV 00. Las Vegas, Nevada: Bechtel SAIC Company. ACC: DOC.20030404.0004.

163045 BSC 2003. *UZ Flow Models and Submodels*. MDL-NBS-HS-000006 REV 01. Las Vegas, Nevada: Bechtel SAIC Company. ACC: DOC.20030818.0002.

163228 BSC 2003. *Radionuclide Transport Models Under Ambient Conditions.* MDL-NBS-HS-000008 REV 01. Las Vegas, Nevada: Bechtel SAIC Company. ACC: DOC. 20031201.0002.

164889 BSC 2003. *Drift-Scale Radionuclide Transport*. MDL-NBS-HS-000016 REV 00. Las Vegas, Nevada: Bechtel SAIC Company. ACC: DOC.20030902.0009.

162730 BSC 2004. *Particle Tracking Model and Abstraction of Transport Processes.* MDL-NBS-HS-000020 REV 00. Las Vegas, Nevada: Bechtel SAIC Company. ACC: DOC.20040120.0001.

141418 CRWMS M&O (Civilian Radioactive Waste Management System Management and Operating Contractor) 2000. *Particle Tracking Model and Abstraction of Transport Processes.* ANL-NBS-HS-000026 REV 00. Las Vegas, Nevada: CRWMS M&O. ACC: MOL.20000502.0237.

151940 CRWMS M&O 2000. *Unsaturated Zone Flow and Transport Model Process Model Report.* TDR–NBS–HS–000002. REV 00, ICN02. Las Vegas, Nevada: ACC: MOL.20000831.0280.

100569 Domenico, P.A. and Schwartz, F.W. 1990. *Physical and Chemical Hydrogeology*. New York, New York: John Wiley & Sons. TIC: 234782.

160844 Feder, J. 1988. *Fractals*. New York, New York: Plenum Press. TIC: 253584.

162573 Goode, D.J. 1996. "Direct Simulation of Groundwater Age." *Water Resources Research, 32*, (2), 289-296. Washington, D.C.: American Geophysical Union. TIC: 252291.

163236 Hogg, R.V. and Craig, A.T. 1978. *Introduction to Mathematical Statistics*. 4th Edition. New York, New York: Macmillan. TIC: 254311.

147209 Kazemi, H. and Gilman, J.R. 1993. "Multiphase Flow in Fractured Petroleum Reservoirs." Chapter 6 of *Flow and Contaminant Transport in Fractured Rock*. Bear, J.; Tsang, C-F.; and de Marsily, G., eds. San Diego, California: Academic Press. TIC: 235461.

144612 LeCain, G.D.; Anna, L.O.; and Fahy, M.F. 2000. *Results from Geothermal Logging, Air and Core-Water Chemistry Sampling, Air-Injection Testing, and Tracer Testing in the Northern Ghost Dance Fault, Yucca Mountain, Nevada, November 1996 to August 1998*. Water-Resources Investigations Report 99-4210. Denver, Colorado: U.S. Geological Survey. TIC: 247708.

116797 Lin, M.; Hardy, M.P.; and Bauer, S.J. 1993. *Fracture Analysis and Rock Quality Designation Estimation for the Yucca Mountain Site Characterization Project*. SAND92-0449. Albuquerque, New Mexico: Sandia National Laboratories. ACC: NNA.19921204.0012.

105729 Liu, H.H.; Doughty, C.; and Bodvarsson, G.S. 1998. "An Active Fracture Model for Unsaturated Flow and Transport in Fractured Rocks." *Water Resources Research, 34*, (10), 2633-2646. Washington, D.C.: American Geophysical Union. TIC: 243012.

160849 Neuman, S.P.; Illman, W.A.; Vesselinov, V.V.; Thompson, D.L.; Chen, G.; and Guzman, A. 2001. "Lessons from Field Studies at the Apache Leap Research Site in Arizona." Chapter 10 of *Conceptual Models of Flow and Transport in the Fractured Vadose Zone*. Washington, D.C.: National Academy Press. TIC: 252777.

159538 NRC (U.S. Nuclear Regulatory Commission) 2002. *Integrated Issue Resolution Status Report*. NUREG-1762. Washington, D.C.: U.S. Nuclear Regulatory Commission, Office of Nuclear Material Safety and Safeguards. TIC: 253064.

165171 Reamer, C.W. 2001. U.S. Nuclear Regulatory Commission/U.S. Department of Energy Technical Exchange and Management Meeting on Total System Performance Assessment and Integration (August 6 -10, 2001). Letter from C.W. Reamer (NRC) to S. Brocoum (DOE/YMSCO), August 23, 2001, with enclosure. ACC: MOL.20011029.0281.

161654 Wang, J.S. 2003. "Scientific Notebooks Referenced in Model Report U0090, Analysis of Hydrologic Properties Data, MDL-NBS-HS-000014 REV00" Memorandum from J.S. Wang (BSC) to File, February 10, 2003, with attachments. ACC: MOL.20030306.0535.

155770 Wang, Z.; Feyen, J.; and Elrick D.E. 1998. "Prediction of Fingering in Porous Media." *Water Resources Research, 34*, (9), 2183-2190. Washington, D.C.: American Geophysical Union. TIC: 250733.

160843 Yamamoto, H.; Kojima, K.; and Tosaka, H. 1993. "Fractal Clustering of Rock Fractures and Its Modeling Using Cascade Process." *Scale Effects in Rock Masses, (Proceedings of the Second International Workshop on Scale Effects in Rock Masses, Lisbon, Portugal, June 25, 1993)*. da Cunha, P., ed. Pages 81-86. Rotterdam, The Netherlands: A.A. Balkema. TIC: 253608.

160839 Yang, I.C. 2002. "Percolation Flux and Transport Velocity in the Unsaturated Zone, Yucca Mountain, Nevada." *Applied Geochemistry, 17*, (6), 807-817. New York, New York: Elsevier. TIC: 253605.

C.5.2 Software Codes

165741 LANL (Los Alamos National Laboratory) 2003. *Software Code: FEHM*. V2.21. SUN, SunOS 5.8; PC, Windows 2000 and Linux 7.1. 10086-2.21-00.

146654 LBNL (Lawrence Berkeley National Laboratory) 1999. *Software Code: T2R3D*. V1.4. FORTRAN 77, SUN, DEC/ALPHA. 10006-1.4-00.